

SELF-RECONFIGURABLE MODULAR EXOSKELETON

A THESIS SUBMITTED TO  
THE GRADUATE SCHOOL OF NATURAL AND APPLIED SCIENCES  
OF  
MIDDLE EAST TECHNICAL UNIVERSITY

BY

ÇAĞRI ALTINTAŞI

IN PARTIAL FULFILLMENT OF THE REQUIREMENTS  
FOR  
THE DEGREE OF THE MASTER OF SCIENCE  
IN  
ELECTRICAL AND ELECTRONICS ENGINEERING

MAY 2014



Approval of the thesis:

**SELF-RECONFIGURABLE MODULAR EXOSKELETON**

submitted by **ÇAĞRI ALTINTAŞI** in partial fulfillment of the requirements for the degree of **Master of Science in Electrical and Electronics Engineering Department, Middle East Technical University** by,

Prof. Dr. Canan Özgen  
Dean, Graduate School of **Natural and Applied Science**

\_\_\_\_\_

Prof. Dr. Gönül Turhan Sayan  
Head of Department, **Electrical and Electronics Eng.**

\_\_\_\_\_

Prof. Dr. Aydan M. Erkmén  
Supervisor, **Electrical and Electronics Eng. Dept. METU**

\_\_\_\_\_

**Examining Committee Members:**

Assoc. Prof. Dr. Uluç Saranlı  
Electrical and Electronics Eng. Dept., METU

\_\_\_\_\_

Prof. Dr. Aydan M. Erkmén  
Electrical and Electronics Eng. Dept., METU

\_\_\_\_\_

Prof. Dr. Osman Parlaktuna  
Electrical and Electronics Eng. Dept., Eskişehir  
Osmangazi University

\_\_\_\_\_

Assoc. Prof. Dr. Umut Orguner  
Electrical and Electronics Eng. Dept., METU

\_\_\_\_\_

Assoc. Prof. Dr. Emre Tuna  
Electrical and Electronics Eng. Dept., METU

\_\_\_\_\_

**27.05.2014**

**I hereby declare that all information in this document has been obtained and presented in accordance with academic rules and ethical conduct. I also declare that, as required by these rules and conduct, I have fully cited and referenced all material and results that are not original to this work.**

Name, Last name : Çađrı ALTINTAŐI

Signature :

## **ABSTRACT**

### **SELF-RECONFIGURABLE MODULAR EXOSKELETON**

ALTINTAŞI, Çağrı

M.Sc., Department of Electrical and Electronics Engineering

Supervisor: Prof. Dr. Aydan M. Erkmén

May 2014, 108 pages

Exoskeleton robot is a supporting structure for soldiers to lighten the weight of their equipment and for people who suffer from medical problems such as lifting, walking etc. This study, the aim is to design an exoskeleton robot for arm that consists of finite self-reconfigurable modular robots, where each modular robot have connections to neighbor modular robots. Firstly, finite element method is used to calculate the stress at each connection. This is followed by the system making a decision by itself on which modular robots will break and where these modular robots will re-connect in the structure, decreasing the stress by utilizing graph theory method. In this thesis, the modeling exoskeleton and the stress analyses have been execute by using Ansy software. Then the obtained results are transferred to Matlab, and it is determined which node will separate itself.

Also, in this thesis, a real exoskeleton robot for assisting the load lifting is designed. This exoskeleton robot can lift a certain level of weight. If the system is overloaded, the least important module within the exoskeleton robot is slid to the point where the load is at highest level.

**Keywords:** Exoskeleton Robot, Graph Theory, Self-Reconfigurable Holonic Robots

## ÖZ

### KENDİNİ TEKRAR ŞEKİLLENDİREBİLEN MODÜLER DIŞ İSKELET ROBOTU

ALTINTAŞI, Çağrı

Yüksek Lisans, Elektrik-Elektronik Mühendisliği Bölümü

Tez Yöneticisi: Prof. Dr. Aydan M. Erkmen

Mayıs 2014, 108 sayfa

Dış iskelet robot, askerlerin yükünü azaltmak ve fazla yük kaldıramayan ya da yürüyememe gibi medikal sorunu olan insanlarda destekleyici bir yapıdır. Bu çalışmada kol için birçok kendi kendine şekillenebilen modüler robotların oluşturduğu bir dış iskelet tasarlanmıştır. Her bir modüler robot, kendisine komşu olan diğer modüler robotla bir bağlantısı vardır. Kola dışardan bir kuvvet uygulandığı zaman, sonlu eleman metoduyla her bir bağlantıdaki gerilmeler hesaplanır. Daha sonra da graf teori metoduyla da sistem kendi kendine hangi modüler robotun kopacağına ve bu kopan modüler robotun, bağlantı noktalarındaki gerilmeyi azaltacak şekilde, nereye tekrar bağlanacağına karar verecektir. Bu tezde exoskeleton modellenmesi ve stress analizleri Ansy programı kullanılarak yapılmıştır. Daha sonra elde edilen sonuçlar Matlaba aktarılarak kopacak olan nod belirlenmiştir

Ayrıca bu çalışmada kol için yük kaldırmaya yardımcı, gerçek bir dış iskelet robotu tasarlanmıştır. Bu dış iskelet robotu belirli bir yükü kaldırabilmektedir. Eğer sisteme

kaldırabileceğinden daha fazla yük uygulanmış ise dış iskelet robotu kendi içerisinde en az öneme sahip olan modülü yükün fazla olduğu bölgeye kaydırarak yükü kaldırmaya çalışmaktadır.

**Anahtar Kelimeler:** Dış İskelet Robotları, Graf Teorisi, Kendi Kendini Şekillendirebilen Modüler Robotlar

To My Family

## ACKNOWLEDGMENTS

I would like to express my sincere appreciation to my supervisor Prof. Dr. Aydan M. Erkmén for her endless support, valuable guidance, and patience throughout this study.

I would especially thank to Dr. Sedat Doğru for his supports, helps and valuable guidance during this study especially during the hardware implementation.

I would like to thank Assist. Prof. Dr. Sebahattin Topal, Assist. Prof. Dr. Umut Tilki, Assist. Prof. Dr. Akif Durdu, Assist. Prof. Dr. Barış Özyer for their supports during the study.

I would like to express my sincere thanks to my father, mother and my brother for their endless support during my life.

## TABLE OF CONTENTS

ABSTRACT.....	v
ÖZ.....	vii
ACKNOWLEDGMENTS .....	x
TABLE OF CONTENTS .....	xi
LIST OF TABLES .....	xiii
LIST OF FIGURES .....	xiv
CHAPTERS	
1 INTRODUCTION .....	1
1.1 Motivation .....	4
1.2 Objectives .....	5
1.3 Contribution of the Thesis .....	6
1.4 Methodology .....	7
1.5 Outline of the Thesis .....	7
2 LITERATURE SURVEY .....	9
2.1 Exoskeleton Robot .....	9
2.1.1 History of Exoskeleton .....	9
2.1.2 Human Augmentation Exoskeletons .....	10
2.1.3 Rehabilitation and Medical Assistance .....	14
2.1.4 Actuating System .....	18
2.2 Modular Self-Reconfigurable Robots .....	19
2.2.1 Control Architectures .....	24
2.3 Mathematical Background .....	28
2.3.1 Graph Theory .....	28
2.3.2 Finite Element Method .....	31
3 METHODOLOGY FOR SELF RECONFIGURABILITY in a MODULAR EXOSKELETON .....	37

3.1	The Holonic Mesh .....	37
3.2	Decentralized Estimation of Exoskeleton Configuration .....	39
3.2.1	Example of Configuration Estimation .....	44
3.3	Self-Reconfiguration .....	45
3.3.1	Determining the Idle Holons: Disconnecting Decision Processes.....	45
3.3.2	Reconfiguration to Provide Support to Exoskeleton Failure under Excessive Load: Reconnection Decision Process.....	47
4	RECONFIGURATION RESULTS AND DISCUSSIONS .....	51
4.1	Checking the Compatibility of the Modular Exoskeleton to the Bending of a Human Arm .....	53
4.2	Experiment 1: Reconfiguration Sequences with Applying Load on One Node	56
4.3	Experiment 2: Reconfiguration Sequences with Applying Load on Two Nodes .....	62
4.4	Sensitivity Analysis .....	74
4.4.1	Relationship between Force and Stress.....	75
4.4.2	Reconnection Criteria .....	76
4.4.3	Increasing Mesh Numbers .....	79
4.4.4	Stress Distributions with Including the Mass of Nodes.....	81
5	HARDWARE IMPLEMENTATION.....	83
5.1	Experiment 1: Exoskeleton Structure with 10 Nodes.....	84
5.2	Experiment 2: Exoskeleton Structure Supporting Arm.....	90
6	CONCLUSION AND FUTURE WORK .....	99
6.1	Conclusions .....	99
6.2	Further Recommendations.....	100
	REFERENCES.....	103

## LIST OF TABLES

### TABLES

Table 3.1 Distributed Procedure(Durna et. al.,2000) .....	42
Table 3.2 Computer Simulation of the Distributed Procedure(Durna et. al.,2000) ..	43
Table 3.3 Procedure 1(Durna et. al.,2000) .....	43
Table 3.4 Current Configuration Estimation Based on Adjacency Matrix .....	44
Table 3.5 Reconfiguration Estimation Based on Stress Matrix .....	46
Table 3.6 Total Principle Eigenvector Component Obtained from Table 3.4 and Table 3.5.....	48
Table 4.1 Properties of Nodes and Elements .....	52
Table4.2 Principle Eigenvector Values for Each Idle Nodes at Each Reconfiguration Sequence .....	62
Table 4.3 Principle Eigenvector Values for Each Idle Nodes at Each Reconfiguration Sequence .....	74
Table 5.1 Properties of Modules .....	83

## LIST OF FIGURES

### FIGURES

Figure 2.1 Hardiman Exoskeleton (Corliss, et. al.,1968).....	10
Figure 2.2 DARPA Lower Exoskeleton (Lenzo, 2013) .....	11
Figure 2.3 BLEEX (Zoss et. al.,2006).....	12
Figure 2.4 HAL Exoskeleton (Sankai, 2011).....	13
Figure 2.5 Body Extender (Marchesci et. al.,2011) .....	13
Figure 2.6 T-Wrex Exoskeleton (Sanchez et. al.,2006) .....	14
Figure 2.7 MGA Exoskeleton (Lenzo, 2013).....	15
Figure 2.8 LOPES Exoskeleton (Veneman et. al.,2007).....	16
Figure 2.9 eLEGS Exoskeleton (Lenzo, 2013) .....	16
Figure 2.10 RUPERT Exoskeleton (Kim, 2012).....	17
Figure 2.11 L-EXOS Exoskeleton (Frisoli et. al.,2009).....	18
Figure 2.12 Self-Organization from Initial to final Configuration (Murata et.al.,1994) .....	21
Figure 2.13 The Connection Types (Murata et. al., 1994) .....	22
Figure 2.14 The Type Transition Diagram (Murata et. al., 1994).....	22
Figure 2.15 An Example to the Fractum Structure Representation (Murata et. al.,1994).....	23
Figure 2.16 Atron System (Yim et. al.,2007).....	27
Figure 2.17 Two Modules Configuration Based on Graph Theory (Baca et. al.,2008) .....	27
Figure 2.18 A Graph Representation.....	28
Figure 2.19 Line Graph of the Graph in Figure 2.14 .....	29
Figure 2.20 Relationship between Strain and Stress in Linear Elastic Material .....	33
Figure 2.21 Geometrical Shape of Pipe .....	33

Figure 2.22 Elastic Straight Pipe.....	35
Figure 2.23 Pipe Structure with Two Nodes.....	35
Figure 2.24 Stress Analysis of Pipe .....	35
Figure 3.1 The Meshed Exoskeleton Structure That Enwraps Arm .....	37
Figure 3.2 Meshed Exoskeleton Structure .....	38
Figure 3.3 Reconfigured Exoskeleton.....	48
Figure 4.1 Exoskeleton Structure .....	51
Figure 4.2 Stress Distributions While Bending the Elbow Part of the Exoskeleton.	53
Figure 4.3 Stress Distributions While Bending the Wrist in Pitch .....	54
Figure 4.4 Stress Distributions While Bending the Wrist in Yaw .....	54
Figure 4.5 Stress Distributions While Bending the Wrist in Roll.....	55
Figure 4.6 Initial Configuration Exoskeleton with Applying Force on Node 8.....	56
Figure 4.7 First Reconfigured Exoskeleton .....	58
Figure 4.8 Second Reconfigured Exoskeleton .....	59
Figure 4.9 Final Reconfigured Exoskeleton.....	60
Figure 4.10 Final Reconfigured Stress Distributions with Extra load on Node 8.....	61
Figure 4.11 Initial Configuration Exoskeleton with Applying Force on Nodes 2 and 4.....	63
Figure 4.12 First Reconfigured Exoskeleton .....	64
Figure 4.13 Second Reconfigured Exoskeleton .....	65
Figure 4.14 Third Reconfigured Exoskeleton.....	67
Figure 4.15 Fourth Reconfigured Exoskeleton .....	68
Figure 4.16 Fifth Reconfigured Exoskeleton .....	69
Figure 4.17 Sixth Reconfigured Exoskeleton .....	71
Figure 4.18 Final Reconfigured Exoskeleton.....	71
Figure 4.19 Final Reconfigured Stress Distributions with Extra load on Nodes 2 and 4.....	72

Figure 4.20 Reconfigured Stress Distributions with Applying Load on Nodes 2, 4, and 39 .....	73
Figure 4.21 Stress Values of each Node with Different Forces Magnitudes .....	75
Figure 4.22 Stresses-Forces Diagram.....	76
Figure 4.23 Reconnection to Only Two Nodes.....	77
Figure 4.24 Reconnection to Other Node at the Same Area .....	78
Figure 4.25 Reconnection to More Than Three Nodes .....	79
Figure 4.26 Exoskeleton with Increasing Mesh Numbers .....	80
Figure 4.27 Stress Distributions with Including Mass of Nodes.....	81
Figure 5.1 Current Exoskeleton Structure.....	84
Figure 5.2 Exoskeleton with 400gr load .....	85
Figure 5.3 Exoskeleton with 1kg load.....	86
Figure 5.4 Present Torque Values of Each Module .....	86
Figure 5.5 Selecting Disconnected Module .....	87
Figure 5.6 ANSYS Analysis of Exoskeleton Structure.....	87
Figure 5.7 Reconfigured Exoskeleton Structure .....	88
Figure 5.8 Reconfigured Exoskeleton with 400gr load.....	89
Figure 5.9 Present Torque Values of Each Module at Reconfigured Exoskeleton... 89	
Figure 5.10 ANSYS Analysis of Exoskeleton Structure.....	90
Figure 5.11 Upper Part of Our System (Arm Part) .....	91
Figure 5.12 Bottom Part of Our System (Exoskeleton Part).....	92
Figure 5.13 Applying 300 g load on Arm .....	92
Figure 5.14 Present Torque Values on Arm Modules.....	93
Figure 5.15 Applying 300 g load on Arm .....	93
Figure 5.16 Exoskeleton is active to lift weight.....	94
Figure 5.17 Present Torque Values on Arm and Exoskeleton Modules .....	94
Figure 5.18 Applying 2.5kg load on Arm .....	95
Figure 5.19 Present Torque Values on Exoskeleton Modules While Applying 2.5kg Load on Arm .....	96

Figure 5.20 Selecting Disconnected Module for Reconfiguration.....	96
Figure 5.21 Reconfigured Exoskeleton Structure .....	97
Figure 5.22 Reconfigured Exoskeleton with Present Torque Values While Lifting 2.5kg weight.....	97



## CHAPTER 1

### INTRODUCTION

This thesis work is the seminal contribution towards creating a visionary trend in exoskeleton, an intelligent self-reconfigurable mold or cast of a human body.

The reconfigurable mold (RCM) is an “architecture machine that produces parts that can be combined to create more complex organizations. The molds are simple analog computers that employ various continuous scales like volume, weight and heat to develop their unique components.”(Khan, 1970) They take on the problem of designing the “shaping” of a material rather than realization of an instantiation of shapes. They are not representational but full scale prototyping tools that produce parts which are subsequently assembled to make more complex wholes. They address fabrication based on dialogue between materials, designer and the contingencies of production and use heuristic tools as much as possible for making objects. Reconfigurable molds (RCMs) have the capacity to be reshaped to produce a controlled variety of products. They are developed in order to rapidly adjust of production capacity and functionality, in response to new circumstances, by rearrangement or change of its components (Mehrabi et al, 2000). They generate constructs that are more versatile and robust to massively increase productivity by reducing tool costs and creating and lead times by up to 90%. Recent application areas of reconfigurable molds, most suitable to the robotic fields, encompass in majority the aerospace, marine, automotive, etc. (Khan, 1970)

Nowadays wearable molds are nonexistent yet, left alone the reconfigurable wearable ones. The recent literature only abounds of wearable robots which are worn by a human operator and support its operator’s any extremity functions, such as limb or

leg and are controlled generally by the operator (human). When wearable robots can replace limb of any human operator, they enter the field of physical orthotic robots or exoskeletons. They can also be placed as an amputation in order to replace the functions of amputated extremity entering the medical augmentation of human where wearability does not mean that those devices are changeable, portable devices.

Classical exoskeletons are far from the concept of intelligent mold. These exoskeletons use robotic technologies in terms of material, control, sensing and actuating to extend, support, substitute or improve any function and ability of the human limb where it is worn, and also to strengthen or replace any function. In order to classify wearable robots, one should consider the function, which they fulfill in cooperation with its operator. Those robots are classified as follows: (Lenzo, 2013)

**Orthosis** is an externally applied device, which is utilized in order to modify the neuromuscular and skeletal system's structural and functional properties. The reasons of its possible usage are as follows:

- Limiting the movement in certain direction;
- Ensuring the general movement support;
- Providing more work while requiring lower energy;
- Supporting rehabilitation efforts;
- Correcting the shape and/or function of the body,
- Ensuring the smoother movement or less movement-induced pain.

**Prosthetic robot** is an electromechanical system, which replaces a limb after an amputation. Robots having similar properties than the intended externally operated prostheses by the patient and are named electromechanical wearable robotic limbs but also assume active augmentation with the missing functions. Those devices provide the chance to actively compensate the lost functions of operator's missing extremity such as limb. This congestion is provided through the utilization of robotic technology from the aspect of cooperation between operator and robot.

An exoskeleton also exhibits such a cooperation physical and action. This device is an external system having joints and links in order to provide similarities with the human operator. This system is a mechatronic system harmonizing with the human body form and function. Some of the utilization areas of exoskeletons relate to research focusing on telemanipulation, man-amplification, neuro-motor control researches, rehabilitation, and assistive devices providing motor controls to an impaired human.

Exoskeletons can also be classified based on their varying purposes of the used. They encompass the following fields:

**Physiotherapy**, where the operator (patient) uses an exoskeleton to fulfill task-based therapy in either active or passive modes.

**Assistive device**, where the operators is supported in terms of load bearing, and the exoskeleton carries most of the load.

**Haptic device**, where the operator faces physically with virtual objects creating interaction forces. The exoskeleton then transmits the information about object's shape, stiffness, texture, or other properties to user.

**Master device** where the virtual environment is replaced by the actual device and the operator utilizes the exoskeleton in order to manage the robotic system in the teleportation (master/slave) mode. In this case, the exoskeleton transmits the forces created due to the interaction of slave robot and the environment to the operator human.

Our pioneering attempt as a first proof of concept towards an intelligent mold or dynamical cast to be a reconfigurable exoskeleton is the contribution of an intelligent mesh of holonic robotic modules covering the human body or limb to be support mobilized that can reconfigure according to the force distribution over the meshed support. This thesis work provides details of the novel methodology, simulation analysis and physical demonstrative realization of this pioneering approach.

## 1.1 Motivation

Human - Robot cooperation in robot technology has found great importance especially in the field of rehabilitation augmentation of parallelized patients and repetitive works under heavy loads of workers in industry.

Human-Robot interaction in wearable robots, especially equipped with assistance to human power and dexterity, is the representative of future robotic development. Within this scope, because of their main advantages such as operation similarities and singularity avoidance, the robots can replace functions of human limb.

In existing exoskeleton robots, actuators which are able to produce high torques are utilized in order to improve the efficiency of the system (i.e. carrying more weights). But those actuators are heavier than those producing low torques, and this situation leads system to be heavier, and also leads user to carry more load. In addition, actuators producing high torques threaten the human safety. For example; if the actuator in an exoskeleton designed for human arm produces high torque rapidly, it leads the arm to be slid to a certain direction suddenly, and it may lead injuries in that arm.

One of the most critical technology that is a good candidate like in our work to support the need of reconfiguration is reconfigurable swarm robots of recent years. Self-reconfigurable robots are designed of autonomous robot modules, which are capable of connecting and disconnecting and changing colony shape and size in order to adapt to requirements of the medium and task.

The exoskeleton structure created by using self-reconfigurable robots has some advantages. In such systems, the efficiency can be improved via actuators being able to produce less torque. Because, the system can find the point where the load or stress is concentrated, and they can lift the load easily by allocating the unimportant

robots in the system to that location. Another advantage is that the human safety is threatened less because the actuators creating lower torques are used.

These resides behind the main motivation of our focus on generating and advancing self-reconfigurable modular exoskeleton technology.

## **1.2 Objectives**

The specific motivation that swarm-formation control offers in their own field. For us, resides in the online adaptability that help benefit in our work the tailoring of exoskeleton continuously responding to new task and strength distribution needs. Our objective in this thesis aims at handling a totally distributed modular self-organizing exoskeleton. A reconfigurable holonic upper limb exoskeleton that reconfigures based on decisions of disconnection and reconnection when new stress distributions occur at exoskeleton nodes (holons) beyond the acceptable limits of the previous configuration is the more concise summary of our aim and accomplishment. Thus, our new framework is a self-tailoring adaptable exoskeleton made up of identical holonic robots assembled as a reconfigurable meshed network. Once a mesh configuration is attained, the exoskeleton assumes its conventional mission of relieving passively, each module acting as an elastic linear actuator, some weight from joints of a person's arm making the human joint efforts affordable. However variations in human joint loadings during the execution of any job, can easily lead a particular human arm joint to being overloaded beyond its natural limit. The intelligent reconfiguration control of the meshed robot network is then triggered in a decentralized way by deciding upon most 'idle' holons together with the most 'critical' ones of the exoskeleton under new load conditions. The next phase of the decision is carried out determining which one of the holons needs to disconnect and where it needs to reconnect to enhance rigidity. In a holonic exoskeleton structure, the main functional property of the components is their cooperation ability while

keeping their independency. Each holon (node) in the structure is functional to some limited extent since it is an elastic linear actuator and has to cooperate with others. Thus the specific goals of the thesis are to:

1. Generate a decentralized meshed model of the holonic exoskeleton.
2. Evaluate the support distribution for the human arm at rest at the initial tailoring of the exoskeleton to the human in question.
3. Evaluate the force distributions on each holon (node) at any task instant of the exoskeleton supporting the human.
4. Decide if reconfiguration is needed checking the natural limits at each node.
5. Determine the idle holons at that task instant.
6. Generate the location of the most favorable idle holon to relieve the overloaded nodes to establish a better instantiated tailoring of the exoskeleton to the specific demands of the task.

### **1.3 Contribution of the Thesis**

The main contributions of this thesis are:

1. Generating the intelligent mesh concept of a holonic reconfigurable exoskeleton.
2. Developing the autonomous decision process in order to determine idle and critical holons for self-reconfiguration. This process carries out decision about which idle holon to disconnect and where to reconnect on the new configuration with the aim of optimizing force distribution on joints.
3. Designing a simple demonstrative hardware application.

## **1.4 Methodology**

The self-reconfigurable exoskeleton is a structure consisting of connected modular robots, and the style of that connection creates its kinematic properties, creating a “robot network”. The type of highly connect holonic robots forming the intelligent mesh can be represented by an incidence matrix where graph theoretic methods can naturally be implemented. Graph Theory is a well-established theory within the branch of Combinatorics that well suits in the formalism of control of discrete configuration changes. The meshed exoskeleton configuration is first represented as a graph model where we handle the problem of self-reconfigurable as a perturbation of the graph starting from an initial one, reaching a desired target graph presentation. Conversion are utilized for the holonic configuration in a graph representation. First, defining the connection sites as the nodes, and representing each holon as a node and defining the connections between them by existence of links. Moreover, force distributions over changing mesh structures are best evaluated via Finite Element Method once forces are observed (measured) at joints according to their individual sensor tolerances. Here Finite Element Method gives us advantage to divide whole structure into smaller pieces, so it makes easier to analyze stress on each link

## **1.5 Outline of the Thesis**

This paper is organized into 5 main sections. Chapter 1 introduces the main theme and essential contributions of the thesis, while specifying our objective and the motivation behind our aim.

Chapter 2 gives literature reviews of related works.

Chapter 3 provides the infrastructure of the intelligent holonic mesh, which configures achieving a certain equilibrium that exhibits convergent stress distributions evaluated based on finite element method. In addition, this chapter dwells with the intelligent graph theoretic self-reconfiguration that analytically decides which holons have to disconnect and be moved to joints for reconnection in order to provide extra support for that joint.

Chapter 4 provides simulations, hardware results, and sensitivity analysis evaluating the reconfiguration performance of the system.

Chapter 5 provides hardware implementations results

Chapter 6 concludes the thesis also projecting into the future.

## CHAPTER 2

### LITERATURE SURVEY

This chapter focuses on the related works on exoskeleton robot, self-reconfigurable modular robots and introduces an overview of the mathematical background necessary for our theoretical approach.

#### 2.1 Exoskeleton Robot

##### 2.1.1 History of Exoskeleton

US Department of Defense has started a research on a strengthened wearable armor, which can amplify the physical abilities of soldiers in early 1960s. In 1962, there was a study in Air Force's Cornell Aeronautical Laboratory on the feasibility of a master-slave robotic system's utilization as a man-augmentation. In one of those studies, Cornell has found that an exoskeleton, which is a robotic system having significantly less degree of freedom (DOF) than human but having the same visual appearance with human extremity, can fulfill many of requested tasks. General Electric has carried out a research on a man-augmentation system between 1960 and 70, where master-slave system generated has been named Hardiman as an abbreviation of Human Augmentation Research and Development Investigation (Figure 2.1), (Corliss, et. al.,1968; Lenzo, 2013) consisting of overlapping exoskeletons worn by the operator. Besides the advantages it offers, there are also some practical

limitations. For example, as of the year of 1970, the system developed could carry almost 370 kg but the weight of system was 750 kg. Besides the important developments, there were also some technological deficiencies. For example, the computers were not fast enough to control the suit for smooth responds; energy supplies were too large and heavy; the exoskeleton's electromechanical muscles were excessively slow, weighty and bulky.



Figure 2.1: Hardiman Exoskeleton (Corliss, et. al.,1968)

### **2.1.2 Human Augmentation Exoskeletons**

A research of DARPA develops exoskeletons, which would be utilized by soldiers and other personnel carrying heavy packs and equipment. It resulted in a prototype of lower leg device with using DC motors. (Dollar et. al.,2008; Lenzo, 2013), (Figure 2.2). The weight of its prototype is almost 11.8 kg and utilizes the 48 V battery pack. Tests have been carried out, and it has been seen that even though the load on operator's back has seriously decreased, the oxygen consumption of operator has

increased 10% depending on the extra effort required in order to compensate for gait interference.



Figure 2.2: DARPA Lower Exoskeleton (Lenzo, 2013)

The next form of exoskeletons were based on closer human-robot relationships focusing upon on force signals, which represented the user's control on robot. This advance in control issues provided chance for users to establish more precious control on exoskeleton (Kazerooni, 2005; Zoss et. al.,2005, 2006). The Berkeley Lower Extremity Exoskeleton (BLEEX), which is shown in Figure 2.3, is a successful example of exoskeletons from the DARPA projects, and has its own power resource. The designs of its kinematics and operation schemes have been prepared by evaluating the human movement analyses (Zoss et. al.,2005). The main advance in BLEEK is to provide a system creating its own energy autonomously. The design of hybrid hydroelectric portable power supply is another important improvement (Zoss et. al.,2006). For improving the responses of lower limb exoskeleton to users' forces and torques, BLEEX process sensory information from the exoskeleton.

The aim of the Robot Suit Hybrid Assistive Limb (HAL) exoskeleton (Figure 2.4) (Sankai, 2011; Lenzo, 2013) was ranging from training doctors and physical therapists to assisting the disabled, that system was allowing staff to carry heavier loads and as an aid in emergency rescues. The weight of the structure is 23 kg, and it utilizes electric motors running from a 100 V AC battery. The duration of battery is approximately 3 hours, but it changes depending on operator's energy expenditure. HAL does not detect the wearer's motion. It utilizes the sensors placed on skin for detecting the voltages related with the brain signals sent to the muscles, they are named myoelectric signals. In this method, the response time is significantly improved. Myoelectric signals' frequency range starts from a couple of Hertz to approximately 300 Hz, while the voltages range from 10mV to 1mV. Another benefit of sensing the myoelectric signals is that people suffering spinal cord injuries or with paralyzed limbs can utilize that suit.



Figure 2.3: BLEEX (Zoss et. al.,2006).

The Body Extender (Figure 2.5) (Marchesci et. al.,2011; Lenzo, 2013) is a wearable robotic device expressly conceived for material handling in unstructured environment. The main aim of that device is to follow the movements of operator's

limb and to magnify the force used by operator. Components of that robotic structure consist of four robotic limbs (2 arms and 2 legs) which are connected to a central unit (backpack). The kinematic properties of those robotic limbs are similar with those of operator's own limbs. That system contains 22 degrees of freedom, and each of them is operated independently via the DC brushed torque motor. Each of those robotic arms has a gripper with one servo-amplified freedom degree.



Figure 2.4: HAL Exoskeleton (Sankai, 2011)



Figure 2.5: Body Extender (Marchesci et. al.,2011)

### 2.1.3 Rehabilitation and Medical Assistance

The Therapy Wilmington Robotic Exoskeleton (T-WREX), (Figure 2.6), (Sanchez et. al.,2006; Housman et. al.,2007)has been manufactured to be a low-cost, passive training device which can be easily adjusted, provide various support levels and quantitative feedback, and allow semi-autonomous arm training. Patients suffering from chronic stroke and having compromised arm function under normal gravity conditions can execute reaching and drawing movements through utilizing T-WREX. Then (Ragonazi et. al.,2011) modified the WREX using elastic actuator. It is an upper-limb orthosis balancing itself according to gravity and designed for children having muscular problems such as muscular dystrophy or spinal muscular atrophy. WREX is generally in connection with a wheelchair or it is directly connected to a body jacket. The elastic operators are used for two issues: ensure softness for the user and accurate torque control.



Figure 2.6: T-Wrex Exoskeleton (Sanchez et. al.,2006)

An example of upper arm exoskeleton robot is the Maryland-Georgetown-Army (MGA) exoskeleton (Figure 2.7) (Lenzo, 2013) which has been designed for

shoulder. That device has five freedom degrees: three joints for shoulder rotation, one for elbow movements, and one for the scapula movements. That device is utilized in order to evaluate the arm strength, speed, and the range of motion via using onboard sensors, and it services for resistance trainer and virtual reality tool purposes during the rehabilitation. The operation can be observed via a computer-based system guided by safety measures.



Figure 2.7: MGA Exoskeleton (Lenzo, 2013)

The easy-to-convert LOPES device (Figure 2.8) (Veneman et. al.,2007) utilizes 2D operated pelvis segment with a leg exoskeleton consisting of 3 operated rotational joints: 2 at the hip and 1 at the knee. Impedance control is utilized in those joints in order to ensure the bilateral mechanical interaction between the operator and the training subject. The device allows both a “patient-in-charge” and “robot-in-charge” mode, in which the robot is controlled either to follow or to guide the patient, respectively. The EMG values have been measured at 8 important muscles of the leg and the results have showed that a free-walk on this system shows similarities with free treadmill walking.

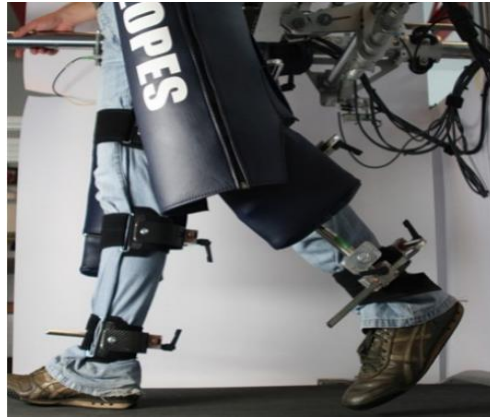


Figure 2.8: LOPES Exoskeleton (Veneman et. al.,2007)

Another wearable exoskeleton system is the Berkeley eLEGS (Figure 2.9) (Strausser et. al.,2011; Lenzo, 2013). In order to detect the operator's gestural intentions, this device utilizes an operator-device interface, which is based on operator's gesture. After detecting the intentions, this device moves in harmony with them. The sensors used in this system works for providing information about the inputs of operator. Through them, even paraplegic operators can walk or move.



Figure 2.9: eLEGS Exoskeleton (Lenzo, 2013)

The RUPERT (Robotic Upper Extremity Repetitive Therapy) as shown in Figure 2.10 was generated in USA as a device focusing on cost-effective therapy for patients [Jiping et. al.,2005; Kim, 2012]. Various prototypes have been developed. In the first generations of this device such as RUPERT RUPERT II, there are 4 pneumatic muscles at the shoulder, elbow and wrist for reinforcing mobility. An adaptable mechanical arm design is also carried out for providing service to various users having various limb dimensions. With this robot, the user is given the chance to satisfy his/her daily requirements such as eating or picking something up from anywhere because of smoothed force support of the device. Controller units are able to be adjusted for users thus improving arm/hand flexibility and strength [Kim, 2012]. The rehabilitation program provided by the exoskeleton is limited to traditional repetitive movement training.



Figure 2.10: RUPERT Exoskeleton (Kim, 2012)

A remote-controlled exoskeleton has been developed for right arms and is named L-Exos (Light Exoskeleton) (Figure 2.11) (Frisoli et. al.,2009; Lenzo, 2013). This device can implement forces lower than 100 N. The force applied can be controlled and the level can be adjusted. This device allows operators to move in any spatial direction and it offers active and reconfigurable arm weight compensation. This system has been designed for easy wearing and usage. That is why; the wrist is

placed at the closed joint and only a therapist is enough for assisting the operator while wearing. The L-Exos device is very suitable for rehabilitation, because there is a tunable height control assistance in this device. The operators can easily fulfill the given tasks because they are given a chair for their comfortable experience.

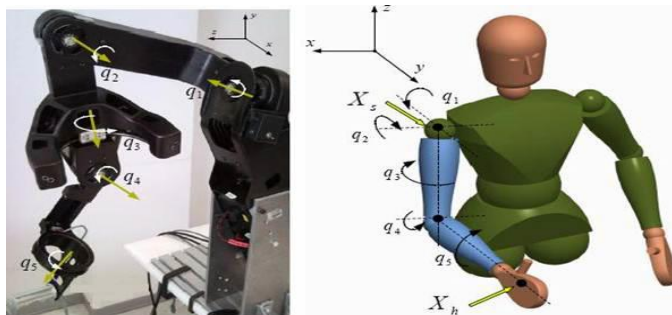


Figure 2.11: L-EXOS Exoskeleton (Frisoli et. al.,2009)

#### 2.1.4 Actuating System

Two main robotic systems are named as active and passive. Because of wide range of kinematic choices, active systems are utilized more widely. But also they have disadvantages such as high energy consumptions (motor operation joints), safety problems of the architecture (for example, any sensor problem may cause instability), fusion difficulties due to excessive number of sensors (Duysinx et. al.,2004; Kikuchi et. al.,2009). For active systems, exoskeletons provide active support to human motion, in many applications surpass human mobility, and are used to guide human such as in rehabilitation applications. On the other hand, passive exoskeletons are always guided by human motion and do not require significant energy. Some of their disadvantages are the possibly limited kinematics, passiveness, and the requirement of manual adjustment (Collins et. al.,2005; Brown, 2011).

Actuation technologies utilized in active robotic systems have been analyzed comparatively in (Hollerbach et. al., 1991). Critical requirements of any actuator in such exoskeletons are its power and lightness. The power and accuracy are the advantages of standard hydraulic cylinders. However, they possess hoses and operating cylinders, which are filled with liquid. That is why; they are very heavy and the liquid may leak onto operator. Another choice of actuation is pneumatics, which utilizes gases. This content makes them excessively unforeseeable. The movement length varies depending on the pressure of gas and the level of reactive force. The last option of electronic servomotors are thought to be operative and powerful, and use permanent magnets and step-down gearing in order to ensure the high-level of torque and responsive movement in a small package. In order to ensure low energy consumption in stand-by position, the geared servomotors may use electronic braking (Lenzo, 2013).

Elastic operators are utilized in order to ensure the softness for the user, and to provide accurate torque control. The reason of utilization of torque control is the action of the elastic element like a natural and compatible torque sensor. The calculation of output torque is made by multiplying the angular displacement of the spring by its stiffness. The result of torque measurement can be utilized as feedback signal.

Our focus in this thesis work is to modularize passive exoskeletons where each modules are elastically driven each.

## **2.2 Modular Self-Reconfigurable Robots**

Self-reconfigurable modular types have not been extensively handled yet in the literature covering exoskeletons. The innovation in our model developed in this

thesis work lies behind the self-reconfigurability of a modular exoskeleton device based on Graph Theory

Modular self-reconfigurable (MSR) robots are defined as systems consisting each of many modules, which can adjust their connections among each other and change their structural form. These modules can be homogenous or heterogenous. The advantages of those robotic systems are (Yim et. al.,2007):

**Sophistication:** Self-reconfigurability makes the robotic system suitable for changing its connections (even disconnecting and then connecting again) in order to adapt to a given task.

**Durability:** Those systems even when considered heterogenous in general, may contain many parts which are similar with each other. This property gives those devices the chance to repair themselves even while operating and also the property of graceful degradation.

**Cost-efficiency:** For MSR systems which contain many parts which are similar to same other, this sameness leads to mass production of those parts and modules, which decreases the unit costs. Also the mass production of those modules gives us the chance to design various robots for various tasks from different assembly of those same modules.

The idea of self-reconfigurable robotic devices dates back to 1970s when a “sudden breakthrough” occurred in computerized machinery technology. In 1980s, Toshio Fukuda has utilized that connection mechanism in CEBOT (the abbreviation of cellular robot) (Fukuda et. al.,1988). The difference between our study and CEBOT lies on the agents used, which move autonomously in CEBOT and are spread on a workspace. CEBOT’s modules are physically separated. Being a mobile agent, a CEBOT needs a ‘3D surface to operate on, however a node in our work operates on the whole structure, where this structure is sufficient to be rooted to the ground from

a single point. In our work, a node moves over the structure, by disconnecting, rotating, translating and connecting itself over the others.

The study having the most similarity with ours is the one of Murata et al. Their starting point is a 2D self-reconfigurable device that they improved to a 3D model. The “fractum” is the unitary robot used in the device. The set of those robots constructs a self-assembling machine and the current focus of the authors is on the re-organization of this machine in certain pattern as seen Figure 2.12

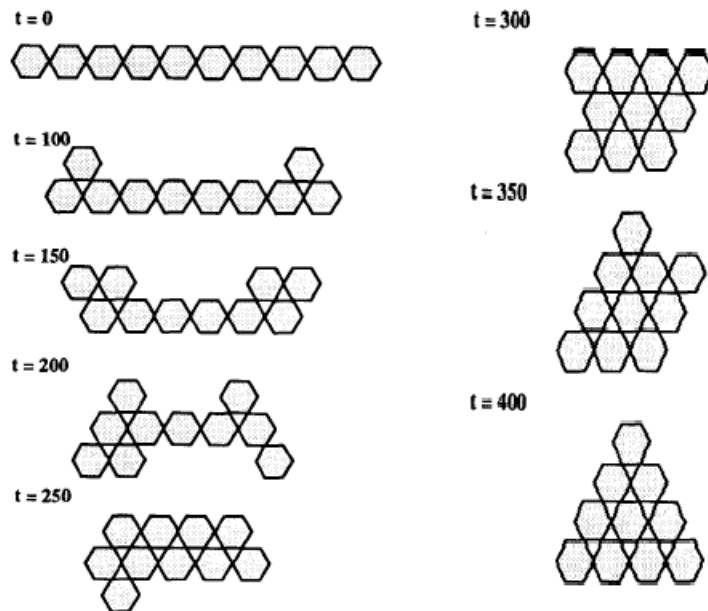


Figure 2.12: Self-Organization from Initial to final Configuration (Murata et.al.,1994)

A decentralized control scheme is then designed that also execute the re-adjustment of the modular system. Murata has considered the universal set of topologically different connection schemas for a Holon(Figure 2.13) and labelled them.

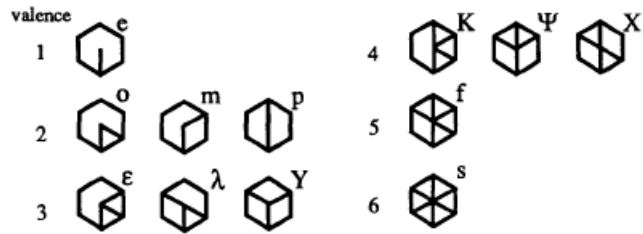


Figure 2.13: The Connection Types (Murata et. al., 1994)

He called the switching pattern between those connection schemes as “Type Transition Diagram” (Figure 2. 14).

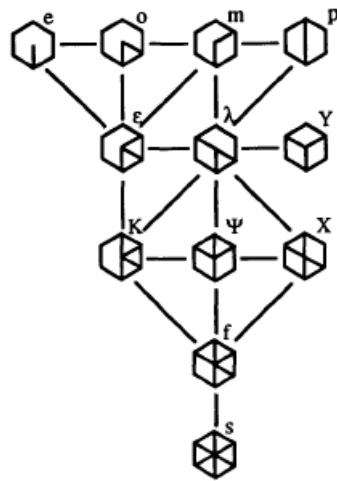


Figure 2.14: The Type Transition Diagram (Murata et. al., 1994)

He used the type labels to represent an assembly. Those labels obtain a list. For example, the configuration in Figure 2.14 can be represented as:

o {K, K}

k {S, K, K, o}

s {K, K, K, K, K,K}

The string in the first line of the given above represents the corner element and its neighbors. The second string is for the side, non-corner fractum, and the last one is for the center fractum and its neighbors.

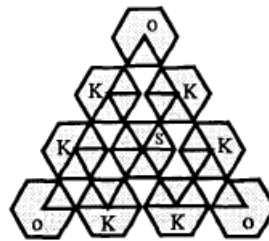


Figure 2.15: An Example to the Fractum Structure Representation (Murata et. al.,1994)

The measure used by each fractum is named fitness which is the distance between actual position in current Configuration State and the final position in the target Configuration State. For computing the fitness, each of fractums uses his neighbors units in the actual configuration and that of the given final one. The value of fitness is calculated as the minimum among all distances. Through that value, it is determined which fractum will move. The motion is determined as a result of comparing the fitness value with an adaptive parameter. The adaptation law is a diffusion formula utilizing local variables from the neighborhood as parameters.

The device developed by (Kurokawa et al. 1998), is again based on grouping the fractum's in different connection patterns. Those labels constitute a lexicon, and

lexicons reflect the image of the general architecture. Decentralized architecture is preferred as a control scheme, and designers utilize the distances as fitness value, in order to make a decision about any motion to be made. The re-adjustment control plan, taking only local variables into account, and utilizing a stochastic relaxation model. This model is based on the distributed Markov Random Field algorithm, and that algorithm is also utilized in parallel optimization problems.

A recent study has designed an exoskeleton named Dual-axis modularized actuator system (DAMA), (Wang et. al.,2011) which has been implemented to humanoid robotic arms. This device consists of two joints operated by a modular two-axis actuator. Two joint modules of DAMA can create high torques. The first joint consists of a harmonic drive, transmission gear (TG), a connector, and a DC motor. This DC motor is placed in the connector, which is also used together with a transmission gear that renders movements more harmonious. In this case, all of the stress components are assessed via finite element analysis. As a result of the analysis, the DAMA device ensures the accuracy of joints through DC motors which are based on PID controller . The main superiority of these modular robots is that each module can connect and disconnect itself to/from its adjacent. However, the main differences from our thesis is our modular robot can moves over the structure and can reconnecting itself over the others.

### **2.2.1 Control Architectures**

Control architectures for modular robotics varies from centralized to decentralized methods. Centralized ones are easy to implement and be analyzed. Corporation burden in decentralized control architecture presents the advantage of being divided over modules sharing this task increasing robustness. Such system can therefore upscale themselves to more modules. The implementation of centralized architecture

utilizing global communications and decentralized architecture utilizing local communication is easier. On the other hand, there also examples of utilization of centralized architecture on a local bus and decentralized architecture on a global bus.

(Yim et. al.,2000, 2007) has applied the centralized control architecture in modular robotic system. In this architecture, there is a controller in each module, manage the position of its local actuator. Besides, the master controller do communicate with module controllers, and manages the local movements such as setting desired joint angles under position control such that the allocated unit transmits the commands to all of individual modules, and synchronizes the movement. The utilization of a *gait control table* is an example of easily applying such centralized control architecture. The gait control table is an  $n \times m$  matrix, where  $m$  indicates the number of modules while  $n$  is the number of steps of the gait. Each cell in the table holds the desired joint angle for a module. Each column of angles corresponds to the sequence of joint angles for a given module. The controller unit reads this matrix row by row, and then transmits the commands to related module. In general, advancing along the table takes certain duration, and the vertical axis represents the duration. The duration between the steps indicates the speed of the joint, and the harmony is ensured by the way.

Enumeration algorithm is another example for centralized control. Chen has developed an enumeration algorithm, which can accurately calculate the number of non-isomorphic configurations in any modular robot (Chen et. al.,1993, Yim et. al., 2007). For determining the number of configurations, structural and kinematic symmetries are used. Polya's Enumeration Theorem is used in this approach for calculating the employed structural only once. For example, any module containing two cubes which has six connection faces has 36 different connection ways. Chen's method regards the 3-fold symmetry of the cubes for calculating that there is only one unique way of connecting the two modules. The assumption in this case is that all of six ports of the cubes are identical. If this assumption is broken, and there are

more than 1 port types (revolute, helical, cylindrical, etc.), this algorithm considers those variations during calculations and this complexity becomes the main disadvantage of the algorithm: the complex nature of the computation yields low performances even for a relatively small problem.

(Rus et. al.,2000, Yim et. al., 2007) has designed a completely decentralized planning system and this algorithm is used after post-cellular-automation (Butler et. al.,2002), model is defined. The cellular automata (CA) management utilized the same rule for all of the modules. The rule can be thought as a group of pre-conditions. If all of the requirements are met, the related action is then implemented. Examples of preconditions can be stated as whether a cell exists at a certain location or not, whether a cell does not exist at a certain location or does, and whether a cell is empty or full. If all of those requirements are met, then the cell acts in a designated direction. Rather than one controller managing the system completely, the modules think for themselves in a decentralized way where the same rule is valid for all of the modules. So the same code is utilized for designing the modules. On the other hand, this control method leads some complexity during developing the arbitrary motions, and its implementation in CA case is also hard to execute.

The unique utilization of Neighbor-to-Neighbor ( $n \times n$ ) communication is seen in ATRON as shown Figure 2.16 (Yim et. al.,2007; Jorgensen et. al.,2004;Rus et. al.,2000). The distributed algorithms utilize processors of the modules which interact harmoniously. In addition, that algorithm then divides the computation which is required for configuration detection and planning the motion. Those MSR devices generally utilize token-type messages. In those messages, a module to another transmits the cumulative configuration data. The main advantage of decentralized architecture is that there is not a requirement of a unique module ID, because each of modules is capable of communicating with its neighbors only. So address space is not a problem anymore. Decentralized approaches also promise to scale as computational resources scale with the number of modules. On the other hand, the

complexity measurement is an important point while distributing the goal configuration detection messages to modules. Planning phase has huge importance even for a couple of modules so this algorithm is suitable for up to 8 modular robots.

The utilization of Graph Theory in modular robotic technology has increased in recent years. A very popular example of MSR robotic systems is named RobMAT (Figure 2.17), (Baca et. al.,2008). In this study, they generate different configurations using modular robots. Kinematic properties of these configurations are obtained by incidence matrices in an edge-oriented graph. From the aspect of Graph Theory, our research and this study have similarity, but the main difference lies behind that this study does not provide any information about self-reconfigurability of their robotic devices.



Figure 2.16: Atron System (Yim et. al.,2007)

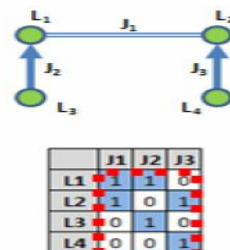
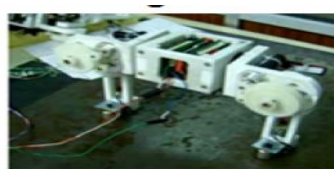


Figure 2.17: Two Modules Configuration Based on Graph Theory (Baca et. al.,2008)

## 2.3 Mathematical Background

### 2.3.1 Graph Theory

A graph is represented by a  $G = (V, E)$

where

- vertex  $V$ , is just a list of indices;
- edge  $E$ , consists of two vertices.

Generally graph can be presented as a consists of vertices and edges as seen Figure 2.18. According the this figure,  $V = \{A,B,C,D,E\}$  is the set of vertices and  $E = \{1,2,3,4\}$  is the set of edges where  $1 = \{A,E\}$ ,  $2 = \{B,E\}$  etc.

A graph is connected if there exist a path between vertices otherwise; it is called as disconnected. The line graph  $L(G)$  of a graph  $G$  is created by allocating the edges of  $G$  as the vertices of  $L(G)$ . This creation would work only if two edges of  $G$  are adjacent to each other, then those vertices would be adjacent to each other in  $L(G)$ . The line graph presentation of Figure 2.18 is given Figure 2.19.

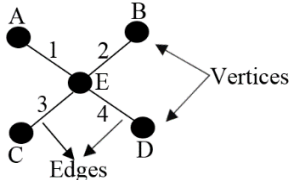


Figure 2.18: A Graph Representation

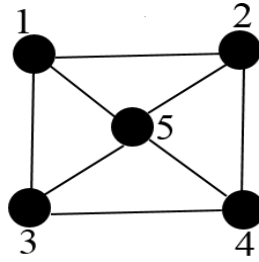


Figure 2.19: Line Graph of the Graph in Figure 2.14

There are various methods for representing any graph. It can be represented in a visual aid diagram, two sets constituting the vertices and edges, a typical polynomial, adjacency matrix or incidence matrix. On the other hand, the unique definition of any given graph can be executed via adjacency matrix. An adjacency matrix  $\mathbf{A}$  of a graph  $G=(V,E)$  with the set  $V$  having a cardinality of  $n$ , is a square matrix of order  $n \times n$ . The definition of adjacency is:

$A = (a_{ij})$ , where  $i, j = 1, \dots, n$ , and  $a_{ij}$  = number of edges from vertex  $i$  to  $j$ . For the graph in Figure 2.14, the adjacency matrix is:

$$A = \begin{pmatrix} 0 & 1 & 1 & 0 & 1 \\ 1 & 0 & 0 & 1 & 1 \\ 1 & 0 & 0 & 1 & 1 \\ 0 & 1 & 1 & 0 & 1 \\ 1 & 1 & 1 & 1 & 0 \end{pmatrix}$$

The graph can also be represented as a *incidence matrix*. Two-type incidence matrix can be appeared: *vertex-edge incidence matrix* and *edge-vertex incidence matrix*. The *vertex-edge incidence matrix*  $\mathbf{R}$  of graph  $G$  that has  $n$  vertices and  $m$  edges and the definition is:

$R = (a_{ij})$   $a_{ij} = 1$ ;  $v_i$  is *incidence with*  $e_j$ , and  $a_{ij} = 0$  otherwise, where  $I = 1, \dots, n$ ,  $j = 1, \dots, m$ ,  $V = \{v_1, \dots, v_n\}$ , and  $E = \{e_1, \dots, e_m\}$ .

For the graph in Figure 2.19, the *vertex-edge incidence matrix* is:

$$\mathbf{R} = \begin{pmatrix} 1 & 0 & 0 & 0 & 0 \\ 0 & 1 & 0 & 0 & 0 \\ 0 & 0 & 1 & 0 & 0 \\ 0 & 0 & 0 & 1 & 0 \\ 1 & 1 & 1 & 1 & 0 \end{pmatrix}$$

The *degree matrix*  $\mathbf{D}$  is the diagonal matrix of graph  $G$  whose  $(i,i)$  entry is the degree of the vertex  $i$  with the off-diagonal entries are equal to zero. The degree matrix of the graph in Figure 2.19 is:

$$\mathbf{D} = \begin{pmatrix} 1 & 0 & 0 & 0 & 0 \\ 0 & 1 & 0 & 0 & 0 \\ 0 & 0 & 1 & 0 & 0 \\ 0 & 0 & 0 & 1 & 0 \\ 0 & 0 & 0 & 0 & 4 \end{pmatrix}$$

The adjacency matrix  $\mathbf{A}(G)$  and  $\mathbf{A}(L(G))$  of a graph  $G$  and  $L(G)$ , vertex-incidence matrix  $\mathbf{R}$  of a graph  $G$  and the matrix  $\mathbf{D}$  of graph  $G$  are related with the:

$$\mathbf{A}(G) = \mathbf{R} \cdot \mathbf{R}^T - \mathbf{D}$$

$$\mathbf{A}(L(G)) = \mathbf{R}^T \cdot \mathbf{R} - 2\mathbf{I} \text{ where } \mathbf{I} \text{ is the identity matrix.}$$

If  $\mathbf{A}$  is the adjacency and square matrix of graph  $G$ , so *characteristic polynomial* of  $\mathbf{A}$  can be found by the following equations:

$$P_A(\lambda) = |\lambda\mathbf{I} - \mathbf{A}|$$

If the roots of the characteristic polynomial of graph  $G$ ,  $P_G(\lambda)$ , are  $\lambda_1, \dots, \lambda_n$  where  $n$  is the vertex number of  $G$ , then  $\lambda_1, \dots, \lambda_n$  call the eigenvalues of  $G$ , and  $\text{Sp}(G) = [\lambda_1, \dots, \lambda_n]$  is the spectrum of  $G$  (Cvetkovic et. al.,1979).

For eigenvalue of  $G$ ,  $A. \bar{x} = \lambda. \bar{x}$  for some non-zero vector  $\bar{x} \in \mathfrak{R}^n$  called the eigenvector of the  $G$ . for an eigenvalue  $\lambda$  of  $G$ , the set  $\{ \bar{x} \in \mathfrak{R}^n \ni A. \bar{x} = \lambda. \bar{x} \}$  defines a subspace of  $\mathfrak{R}^n$ , which is called the eigenspace of  $\lambda$  (Cvetkovic et. al.,1979).

The index is called as the largest eigenvalue of a graph  $G$  and there is a corresponding non-negative eigenvector, which is called the *principal eigenvector* of  $G$ .

### 2.3.2 Finite Element Method

*The finite element method* is a mathematical technique, which is utilized in order to acquire the approximate solutions of complex problems, which cannot be solved via basic theories. The domain of interest is divided by FEM model divides into a finite number of simple sub-domains. In addition, the model utilizes the variation concepts in order to create the estimated solution through sub-domain collection. Those sub-domains are generally named “elements”. That is why; this model is named “Finite Element Method”.

In order to facilitate the analysis, the FEM method disintegrates the structure into the smallest pieces. All of the elements create a “mesh” that can be defined as a problem approximation. Now it is obviously easier to analyze those elements via simple equations for stress. If the number of elements rises, then their size decrease, of course, and the approximate solution theoretically gets more precise.

In FEM, material properties are important to measure stress on each element. The homogenous material can be defined as the pure material that does not include any other material or impurity. Except the composite ones, the materials used in

engineering are mostly accepted to be homogenous ones. For example, if we need steel and we meet this requirement from a dealer, we know that the purchase we bought is pure 99.9%, and it does not contain any trace from other materials. However, non-homogenous material are combine of different materials that effects its yields under stress.

The isotropic material can be defined as the material having the same properties along all dimensions. This principle generally applies to materials, but not to composites or biological materials such as wood or bone. For this type materials, measurement of stress is based on Hooke's law :

$$\sigma = E\varepsilon$$

where

$\sigma$  = stress,

E =Elasticity Constant of Material

$\varepsilon$  = the strain(deformation) of the material

In isotropic material, direction of the load is not important.

The linear elastic material can be described as the basic material type having the widest usage area in stress analyses. The linear elastic material springs in accordance with applied force/load, and then it always returns to its initial position when we stop implementing the force (i.e. obeys Hooke's law). There is no plastic deformation in this material type. In this type material, stress is direct proportion with strain as seen in Figure 2.20.

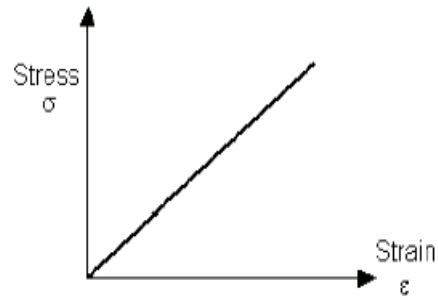


Figure 2.20: Relationship between Strain and Stress in Linear Elastic Material

### 2.3.2.1 Stress Analysis

In this thesis, Linear elastic, isotropic straight pipe is selected as an element type. The geometric shape of this material is given in Figure 2.21.

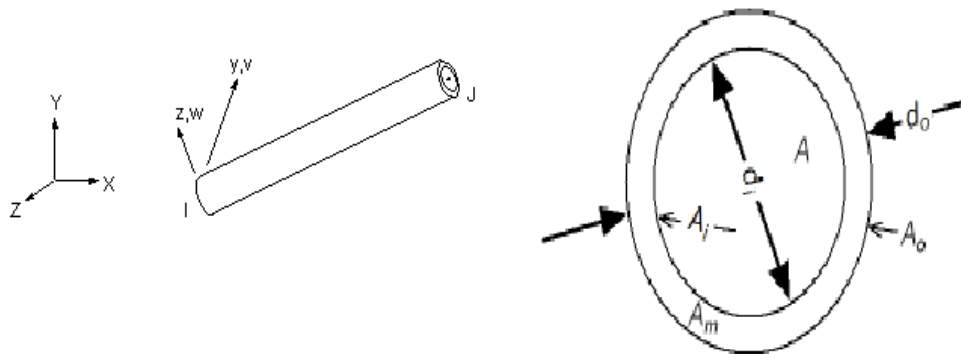


Figure 2.21: Geometrical Shape of Pipe

where

- $D_0$  = Outside Diameter of Pipe
- $D_i$  = Inside Diameter of Pipe and
  - $D_i = D_0 - 2t_w$  where  $t_w$  is the thickness of Pipe

The bending stress is a type of stress occurs when loads are applied perpendicular the on link, forcing it to deflect under the load or pressure. The *stress* calculation of Pipe is:

$$\sigma_{bend} = \frac{M_b r_0}{I_r} \text{ where:}$$

$\sigma_{bend}$  = Bending Stress of Pipe

$M_b$  = Bending Moment

$I_r$  = Bending Moment of Inertia and

- $I_r = \frac{\Pi}{64} [(D_0)^4 - (D_i)^4]$

and  $r_0 = \frac{D_0}{2}$

as a result *stress* is:

$$\sigma_{bend} = \frac{M_b (D_0/2)}{\frac{\Pi}{64} [(D_0)^4 - (D_i)^4]}$$

In the below example we have two nodes and they are homogenous and isotropic. We connect them via elastic straight pipe and the outside diameter of pipe is 30mm, the thickness value is 4mm and the length of the pipe 1 is 400mm as seen Figure 2.22.

As see Figure 2.23, node 1 is selected as a reference frame and 100N force is applied on the node 2 towards the negative y-axis. The stress distribution on the pipe based on node 1 is analyzed by ANSYS and the stress value is 21.2 MPA (Mega Pascal) as shown in the Figure 2.24

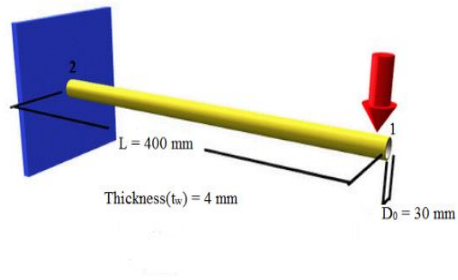


Figure 2.22: Elastic Straight Pipe



Figure 2.23: Pipe Structure with Two Nodes

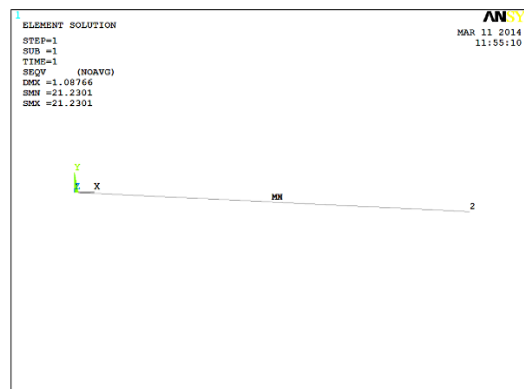


Figure 2.24: Stress Analysis of Pipe

The hand calculation of the stress based on node 1 is:

$$\sigma_{bend} = \frac{M_b (D_0/2)}{\frac{\pi}{64} [(D_0)^4 - (D_i)^4]}$$

where  $D_0 = 30\text{mm}$ ,  $t_w = 4\text{mm}$ ,

$D_i = D_0 - 2t_w = 22\text{mm}$ ,

$M_b = (F_y \times \text{Length}) = 40000(\text{N}\cdot\text{mm})$

so

$$\sigma_{bend} = \frac{40000 \times 15}{\frac{\pi}{64} [30^4 - 22^4]} = 21.2 \text{ MPA}$$

## CHAPTER 3

### METHODOLOGY FOR SELF RECONFIGURABILITY in a MODULAR EXOSKELETON

#### 3.1 The Holonic Mesh

The holonic mesh concept was generated by Durna (Durna et. al.,2000), and in this thesis work, we apply this concept to the formation of a meshed arm exoskeleton composed of rigidly attached holonic robots that enwraps the human arm tightly as see in Figures.3. 1 and 3. 2.



Figure 3.1: The Meshed Exoskeleton Structure That Enwraps Arm

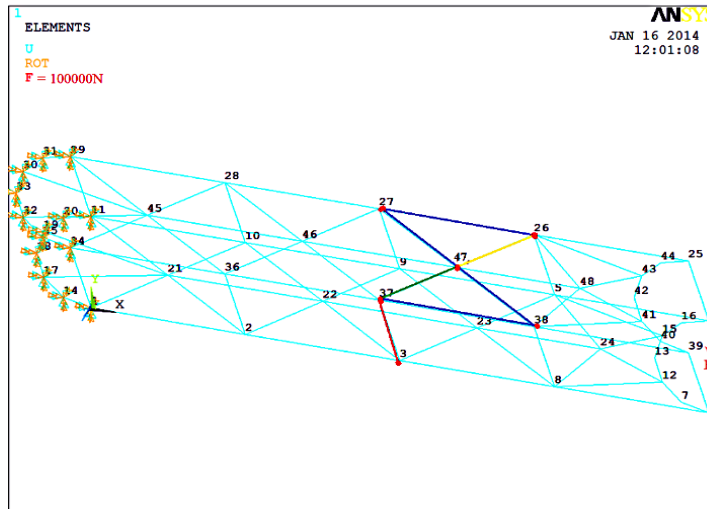


Figure 3.2: Meshed Exoskeleton Structure

This meshed network of homogeneous robots that we developed can decide how to autonomously and dynamically reconfigure in a variety of connection types to realize a certain task and provide robust support to any increase in load. The most important feature of the holonic exoskeleton is that it is formed by homogenous meshes generated by identical holons, each physically connected to a finite number of immediate neighbors forming the vertices of the mesh. Moreover, these holons communicate with their immediate neighbors, from which the communication propagate over the network. In addition, no holon has information about the whole configuration state, however each holon is only informed about the total numbers of holons existent in the structure.

Our objective in this work is to develop a holonic self reconfigurability so that extra support is provided to weak regions of the exoskeleton by idle holons being disconnected from their earlier connections and being connected to the weak area. Thus the critical issues for holons that do not have any information about the whole meshed network structure, is” a systematic approach to make all holons be knowledgeable about the whole meshed network configuration” and answer “how a

holon needs to act to have the reconfiguration of the exoskeleton meet the global need of robustness under loads facing physical limits of certain joints''. We develop our earlier version of answering the first some of those critical questions (Durna et al., 200) based on graph theory technique. However, this earlier version did not consider any self-reconfiguration. In the balance of the thesis, we use the same graph theoretic approach to answer the second question to enable reconfiguration of the holonic exoskeleton, which will be introduced in detail in the coming section.

### **3.2 Decentralized Estimation of Exoskeleton Configuration**

The mesh configuration of an exoskeleton is represented by an adjacency matrix  $A$ . However since each holon does not know about this matrix, this configuration is estimated by the holons through a distributed computation of principle eigenvector components of  $A$  which is a real symmetric matrix diagonalized by the well known similarity transformation;  $U^T A U = \text{diag}(\lambda_1, \lambda_2, \dots, \lambda_n)$ , where  $\lambda_i$  's are the eigenvalues of  $A$  and are called the spectrum of  $A$ . The largest constituent of the spectrum of any matrix is named as Index, and the corresponding eigenvector is named as the principal eigenvector. Our exoskeleton is a graph  $G = (E, V)$ , where  $E$  is the set of edges created by links and  $V$  is the set of vertices which are the holons. It is obvious that such a graph is uniquely defined by its spectrum and eigenspaces (Cvetkovic, 1997).

We will show in this thesis work that the Index and principle eigenvector provide important data about the exoskeleton architecture determining its current configuration.

Each vertex "i" in any exoskeleton such as one in Figure3. 2 has adjacent vertices forming the neighbors of holon i as  $i_1, i_2, i_3$  and  $i_4$  colored in red in this Figure. The

rest of the exoskeleton is named as sub-graphs. In our situation, those are the task environments influenced by the holon  $i$ . So in the  $i^{\text{th}}$  row of adjacency matrix  $A$ , the entries related with neighbors of holon  $i$  take the value of 1, while other entries are zero. Let  $P$  be the vector representing all 48 holons forming the current configuration of the exoskeleton; it is then defined as:

$$P^T = [p_i, p_{i1}, p_{i2}, p_{i3}, \dots, p_{i48}]$$

The multiplication  $AP$  has entries which are each equal to the sum of the values of the neighboring vertices of the vertex  $i$  at the  $i^{\text{th}}$  entry of the outcome vector  $AP$  so that; if vertex  $i$  has 4 neighbors as seen in colored region of Figure3. 2:

$$AP = [\dots, p_{i1} + p_{i2} + p_{i3} + p_{i4}, \dots]^T$$

If  $P$  is an eigenvector then:

$$AP = \lambda P \text{ for } P \neq \bar{0}, P \in \mathfrak{R}^n$$

and the  $i^{\text{th}}$  entry of the  $P$  vector can be written as;

$$\lambda p_i = p_{i1} + p_{i2} + p_{i3} + p_{i4}$$

where  $i_1, i_2, i_3, i_4 \in \{1, 2, \dots, n\}$  for an  $n$  vertex graph.

The holon  $i$  recognizes its role in the configuration by the eigenvector components  $p_{ik}$  of its adjacent  $k$  and the Index  $\lambda$  computed through :

$$p_i(t) = \frac{\sum_{k=1}^4 p_{ik}(t-1)}{\lambda_i(t-1)}$$

$$\lambda = \lim_{t \rightarrow \infty} \lambda_i(t)$$

where  $t$  is the number of iterations. This schema is a **law of coalition** within the colony

This case give opportunity to distributed computation takes the neighborhood of the holonic robot unit  $i$ ,  $i$  varying over the colony and thus recursively finds the eigenvectors and eigenvalues of the whole structure starting from the local ones..

The distributed procedure given in Table 3.1 is used by holon  $i$  whose parametric knowledge about the colony, through the index and principle eigenvector undergo consecutive updates and converge to the representation of the global configuration of the colony.

This algorithm is modified from a local Gauss –Seidel-type iterative procedure used by holon  $i$ . In a Gauss-Seidel relaxation, all the updated and available values of variables are used in the computation of a variable. This gives faster convergence than Jacobi-type relaxation because the possible newest information is used for the next iteration whereas the latter one uses only the last values. This iterative method is of the form:

$$x_i(t+1) = f(x_1(t+1), \dots, x_{i-1}(t+1), x_i(t), \dots, x_n(t)) \quad i = 1, \dots, n$$

And the Jacobian – type iteration can be represented as:

$$x_i(t+1) = f_i(x_1(t), \dots, x_n(t)), \quad i = 1, \dots, n$$

The estimation of the global colony configuration iteratively by individuals of the decentralized exoskeleton colony is as follows: Assume that robot  $i$  has  $k(i)$  neighbors and the neighborhood that it belongs to has the index  $i \lambda$  and the principle eigenvector

$${}^i P = \left[ \dots, {}^i P_{i1}, \dots, {}^i P_{i2}, \dots, {}^i P_i, \dots, {}^i P_{ik_i}, \dots \right]^T$$

The computations done by the holon  $i$  take inputs only from the holons in its neighborhood. The component  ${}^i p_j$  is considered to represent the knowledge of robot  $i$  about holon  $j$ . Similarly  ${}^i \lambda$  is the knowledge of the holon  $i$  about the colony.

Table 3.1: Distributed Procedure(Durna et. al.,2000)

<p>/repeat until the index and principle eigenvector components' rate of changes enter in a predetermined region/repeat for each <math>t</math>/</p> <p>{</p> <p>I. for <math>i = 1</math>: number of nodes(holons)</p> <p>II. for <math>j = 1</math>: number of neighboring nodes</p> <p>III. <math>\lambda^i(t) = \frac{{}^i p_{i1}(t-1) + \dots + {}^i p_{k(i)}(t-1)}{{}^i p_i(t-1)}</math></p> <p>IV. <math>{}^i p_j(t) = \frac{{}^i P_j(t-1) + {}^2 P_j(t-1) + \dots + {}^i P_j(t-1) + \dots + {}^{k(i)} P_j(t-1)}{k(i) + 1}</math></p> <p>V. <math>{}^i P_i(t) = \frac{(k(i) + 1) \cdot {}^i \lambda(t)}{{}^i \lambda(t) + \dots + {}^i \lambda(t) + {}^{k(i)} \lambda(t)} {}^i P_i(t)</math></p> <p>VI. Apply procedure I</p> <p>VII. End</p> <p>}</p> <p>Then normalized the final stage.</p>
---

In addition, the computer simulation of the distributed procedure is given Table 3.2.

Table 3.2: Computer Simulation of the Distributed Procedure(Durna et. al.,2000)

<p>If H is as n-holony:</p> <ol style="list-style-type: none"> <li>i. A is the adjacency matrix of the H.</li> <li>ii. <math>I\bar{D}(i)=[0, \dots, 1, \dots, 0]^T</math> The 1 is the ith entry.</li> <li>iii. <math>k(i)+c=\ I\bar{D}(i).(A+cI)\ _1, c \in \mathfrak{R}</math>.</li> <li>iv. <math>\Gamma=diag(^1\lambda(t), ^2\lambda(t), \dots, ^n\lambda(t))</math>: The diagonal eigenvalue matrix of the indices of cliques of holons 1, 2, ..., n of H.</li> <li>v. <math>P(t)=[^1\bar{p}(t): ^2\bar{p}(t): \dots : ^n\bar{p}(t)]^T</math> where <math>^i\bar{p}(t)</math> is the eigenvector of holon i at time t.</li> </ol>
--

Table 3.3: Procedure 1(Durna et. al.,2000)

<ul style="list-style-type: none"> <li>• For holony H and holon i and j in H and <math>j \neq i</math></li> <li>• {</li> <li>• For holon I and holony H, <math>i \in H</math>, for <math>j \neq i</math> at time t</li> <li>• If <math>d(i, j, H)</math> is not computed yet,</li> <li>• <math>d(i, j, H) = t</math> if <math>P_i^j \neq 0</math></li> <li>• Else proceed to holon <math>j + 1 \neq I</math> in the step 2 of the above algorithm.</li> <li>• }</li> </ul>
--

### 3.2.1 Example of Configuration Estimation

As introduced in chapter 1, the contribution of thesis work is mainly the development of a self-reconfiguration capability of the meshed exoskeleton which configuration prior to reconfiguration is identified through the graph-based analysis provided in the previous section using the principle eigenvector components information communicated to all holons of the network. In this section we will demonstrate the evaluation of this global configuration estimated iteratively and through the propagation over the colony. Consider the holon 47 and its neighbors which are 26, 27, 37 and 38 together with node 3 as colored red in the exoskeleton of Figure 3. 2. In the iterative estimation of this configuration of the exoskeleton, after 200 iterations, all holons obtain upon convergence approximately the same index and principal eigenvector that are the whole colony connectivity representation as given in Table 3.4. From these global values found, node 47 has the highest connectivity (0.5958) as also justified from Figure 3. 2 by its highest number of neighbors. This is a holon that should not disconnect; however, node 3 has the minimum connectivity (0.1676) which means that this robot is loosely connected to the network of the exoskeleton, and therefore can be detached for reconfiguration.

Table 3.4: Current Configuration Estimation Based on Adjacency Matrix

Index	Principal Eigenvector Component					
	3	26	27	37	38	47
2.628	0.167	0.365	0.365	0.440	0.394	0.595

### **3.3 Self-Reconfiguration**

#### **3.3.1 Determining the Idle Holons: Disconnecting Decision Processes**

Whenever an extra force  $\Delta F$  is applied to any joint of the human arm beyond its carrying capacity, the holons in that region detect the loss of rigidity at a certain vicinity of a joint in the human limb equipped with the exoskeleton. The holon colony forming the mesh first run the estimation of current configuration as in section 3.1. Holons (modules of exoskeletons) in this procedure distributively determine the idle holons that can be detached from the mesh and be reattached to one of the holons of the critical region under extra load, using the component values of the principal eigenvector found in the estimation.

Idle holons are those that correspond to low values of principle eigenvector components, together with low stress values of the corresponding principle eigenvector found by configuration estimation using the algorithm introduced in section 3.1. So, to make decision on which robot disconnect, the below procedure is available:

1. Obtaining principle eigenvector values for current estimation configuration based on adjacency matrix.
2. After applying forces, detecting principle eigenvector values for reconfiguration estimation based on stress matrix.
3. Making decision about which robot will be disconnected, system detect an idle holon that has minimum principle eigenvector value according both adjacency and stress matrix. In the structure, if one more nodes have same minimum principle eigenvector values, system choses one of these nodes as

an idle holon randomly. If there is no extra force obtained, go with step 2 else continue with final step.

4. After obtaining the idle holons which will be disconnected, we reconnect it between three nodes; two nodes belong to highest stress link and one node belongs the higher principle eigenvector at this area.

In this thesis, system select idle node automatically, however, disconnecting and reconnecting are made manually.

Therefore we add both principle eigenvector values obtained from adjacency and stress matrix to detect idle holons.

We provide here a simple illustrative example of the reconfiguration procedure. Now consider the exoskeleton in Figure 3.2 where we apply force of 100N in the negative (downward) direction at node 3, and node 26 selected as a reference frame to analysis stress distribution. All stresses at each link in the new loaded configuration are calculated using ANSYS and the maximum stress is found at the link between nodes 3 and 37, which is colored in red and have magnitude of 0.69MPA. However, minimum stress occurs between nodes 27 and 26, which are colored blue as seen in Figure 3.2.

Table 3.5: Reconfiguration Estimation Based on Stress Matrix

Index	Principal Eigenvector Component					
10.8183	3	26	27	37	38	47
	0.94	0.0028	0.0028	0.352	0.0382	0.0017

According to this illustrative example, after 200 iterations, all nodes obtain approximately the same index and principal eigenvector that are the whole colony stresses representation as given in Table 3.5. From these global values found for the whole exoskeleton, node 3 has the highest principle eigenvector (0.94); while, node 47 has the lowest one. According this data obtained from Table 3.5, node 47 see as an idle holon that must be disconnect.

### **3.3.2 Reconfiguration to Provide Support to Exoskeleton Failure under Excessive Load: Reconnection Decision Process**

Node 47 is selected as an idle holon from Table 3.5, however, it has maximum principle eigenvector for current configuration estimation analysis based on adjacency matrix as shown in Table 3.4, and it is chosen as a non-disconnecting robot. Similarly, node 3 in Table 3.4 has minimum principle eigenvector value for current estimation and can be disconnect; on the other hand, according to reconfiguration estimation based on stress matrix, node 3 in Table 3.5 has the maximum principle eigenvector value thus it not be disconnected. Therefore, we have to find an idle holon which has a minimum principle eigenvector for both cases: current estimation and reconfiguration estimation. Therefore, we add both principle eigenvector values obtained from Tables 3.4 and 3.5, and this summation is given in Table 3.6.

According to Table 3.6, nodes 26 and 27 have the minimum principle eigenvector values. In addition, these nodes have minimum ones due to Table 3.4 and Table 3. 5. Thus node 26 and 27 as shown in Table 3.6 are loosely connected (idle holons) to the network and are easily detached for reconfiguration. Idle holons are where disconnection will occur in a previously estimated configuration and will attach to those critical holons under heavy load with stress. Node 26 is selected as a fixed

node therefore we disconnect the node 27 and reconnect the link between nodes 3 and 37; also we connect it to node 38 which has the other node at this area. New configuration is shown in Figure 3.3. Such reconfiguration will thus decrease stress distributions in that reconfigured exoskeleton compared to its previous configuration.

Table 3.6: Total Principle Eigenvector Component Obtained from Table 3.4 and Table 3.5

Total Principal Eigenvector Component					
3	26	27	37	38	47
1.107	0.365	0.365	0.792	0.4322	0.595

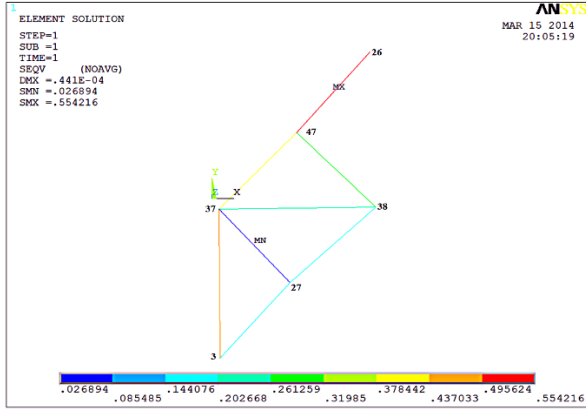


Figure 3.3: Reconfigured Exoskeleton

For the new reconfigured exoskeleton, stress value on the link between nodes 3 and 37 is 0.41MPa, which was 0.69MPa for the previous configuration.

After obtaining this new configuration(k+1), a stress analysis carried to observe if all stress values have been decreased to levels under threshold value at all joints; if it is not the case, a new configuration(k+2) is conducted after that the current configuration(k+1) is again estimated. Such reconfiguration sequences will be illustrated and discussed in chapter 4.



## CHAPTER 4

### RECONFIGURATION RESULTS AND DISCUSSIONS

The meshed holonic network forming the exoskeleton assesses the local stress at each mobile robot node through sensors in actual hardware applications. In these simulation examples, the sensing process is calculated as an input using Ansys. All information obtained from Ansys is transferred to Matlab for decision-making process.

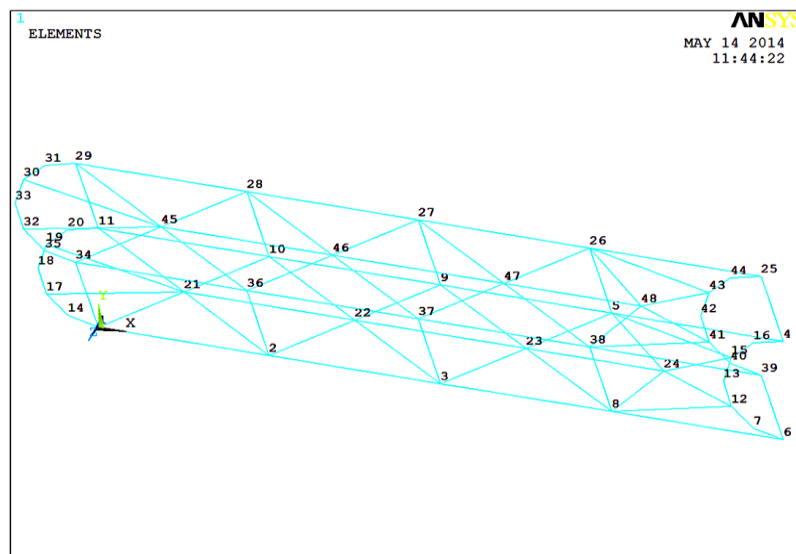


Figure 4.1: Exoskeleton Structure

During the simulations, the structure of our exoskeleton is seen in Figure 4.1. Nodes in the semicircle between nodes 1 and 11 and between nodes 29 and 34 indicate the shoulder part, while the nodes in the semicircle between the nodes 4 and 6 and between nodes 25 and 39 indicate the wrist part. Our exoskeleton have hyper redundancy in the links and nodes. Properties of nodes and elements are given in Table 4.1. The weights of nodes are neglected during the simulation.

Table 4.1: Properties of Nodes and Elements

Node numbers	48
Element Numbers	96
Outside Diameter of Element	40mm
Wall Thickness of Element	10mm
Modules Of Elasticity	1MPA
Stress Handling Capacity	0.8MPA(1/1000000 scaled)

The arm exoskeleton simulated in these experiments has a maximum stress handling capacity of 0.8MPA for each joint where these values have been used with a scale of (1/1000000). Our aim in this simulation experiment of this chapter is to hold all joint stresses well below half of their individual maximum stress capacity.

Fixed nodes are the connection nodes of the exoskeleton to the human arm. Thus in this exoskeleton structure, the fixed nodes are the shoulder connections being the 11<sup>st</sup>, 14<sup>th</sup>, 24<sup>th</sup>, and 29<sup>th</sup> ones located on the semicircle adaptation of the exoskeleton to the human shoulder as seen Figure. 4.1. These nodes are reference frames in stresses distributions analyses. Those fixed nodes are not considered in the

computation of the principle eigenvector since they remain fixed through all reconfigurations. They are not allowed to connect or disconnect.

#### 4.1 Checking the Compatibility of the Modular Exoskeleton to the Bending of a Human Arm

The exoskeleton is fixed at the shoulder while the modules covering the arm become under compression or elongation according to their location along the arm, when the elbow bend and the wrist moves in pitch, yaw and roll conditions.

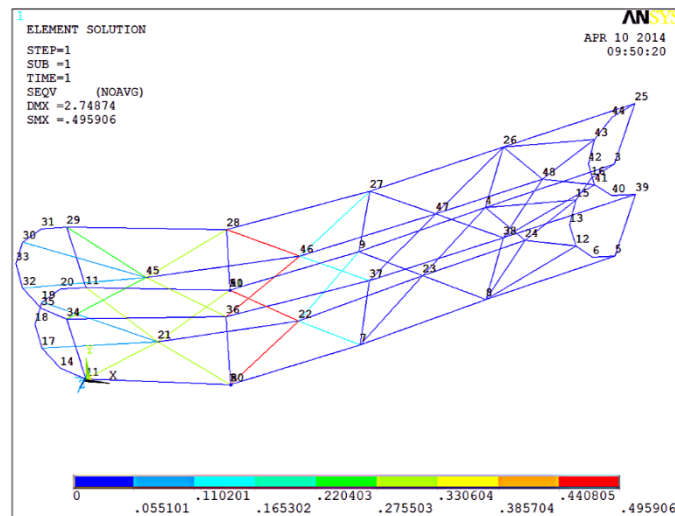


Figure 4.2: Stress Distributions While Bending the Elbow Part of the Exoskeleton

Figure 4.2 shows the stress distributions while human bending elbow part of the arm to natural configuration, maximum stresses (0.49MPa) are occur on the links between nodes 28 and 46, nodes 36 and 46, 22 and nodes, 10 and 22.

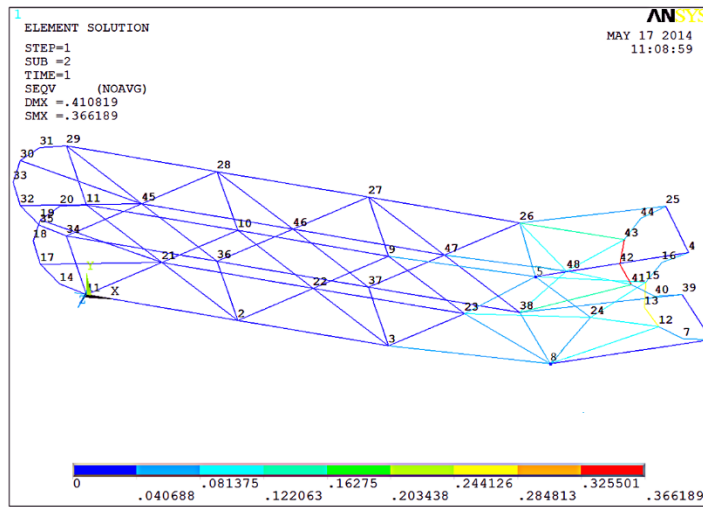


Figure 4.3: Stress Distributions While Bending the Wrist in Pitch

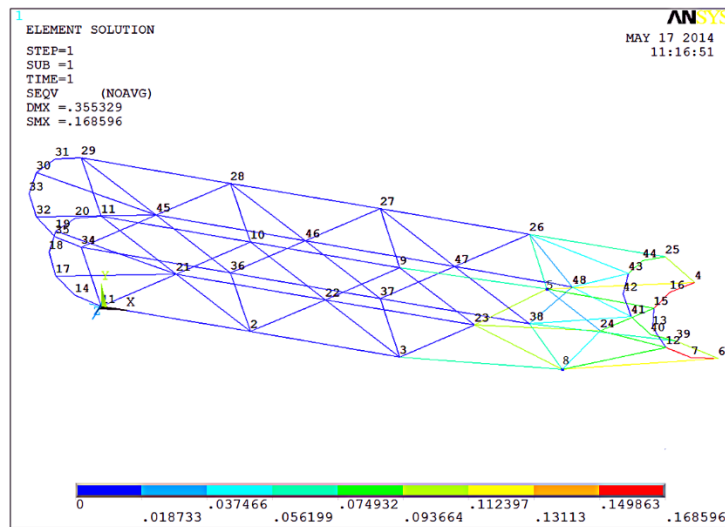


Figure 4.4: Stress Distributions While Bending the Wrist in Yaw

When bending the wrist in pitch, maximum stresses are obtained on the links between nodes 41 and 43, and nodes between 12 and 15 (0.366MPa) as seen Figure 4.3. For the yaw condition, maximum stress are measured (0.17MPa) on the links

between nodes 4 and 15, and nodes 6 and 12 as seen Figure 4.4. And the roll condition for wrist as shown in Figure 4.5 in three frames. According this figure, maximum stress (0.17MPa) are occur on the links between nodes 5 and 6, and nodes 3 and 16.

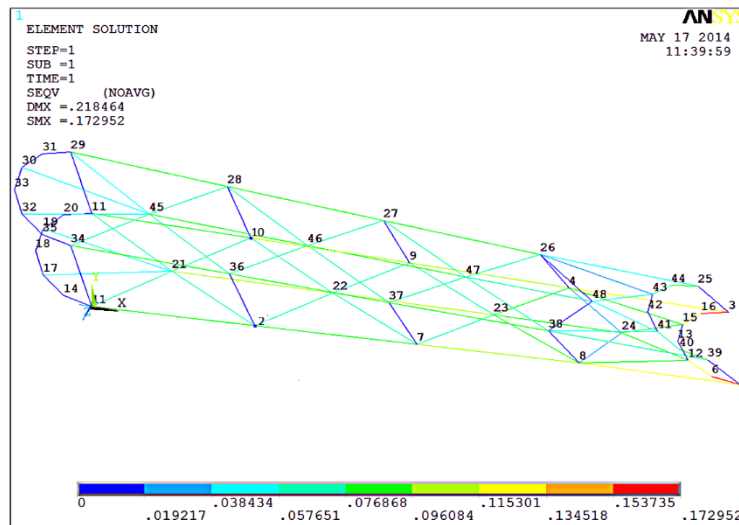


Figure 4.5: Stress Distributions While Bending the Wrist in Roll

All stress distributions on the below figures are lower than the exoskeleton handling capacity (0.8 MPA), so our exoskeleton structure does not require any self-reconfiguration during the bending of the elbow part or wrist in pitch, yaw and roll conditions.

### 4.2 Experiment 1: Reconfiguration Sequences with Applying Load on One Node

In this simulation part, our aim is to hold all joint stresses well below half of their individual maximum stress capacity while applying load on one node.

The principle eigenvector components of every holon based on estimate configuration (adjacency matrix) in the exoskeleton (Figure 4.1) are given in Figure 4.6. The maximum ones are seen to correspond to the 22<sup>nd</sup>, 23<sup>rd</sup>, 46<sup>th</sup> and 47<sup>th</sup> holonic robots. These are nodes with most connections and should never disconnect. Now an extra load of 1000N is applied at the human joint area around the 8<sup>th</sup> node of the exoskeleton in Figure 4.6, which is way beyond the joint limit of the human arm equipped with the previous configuration of the exoskeleton. The force is directed in the negative y direction.

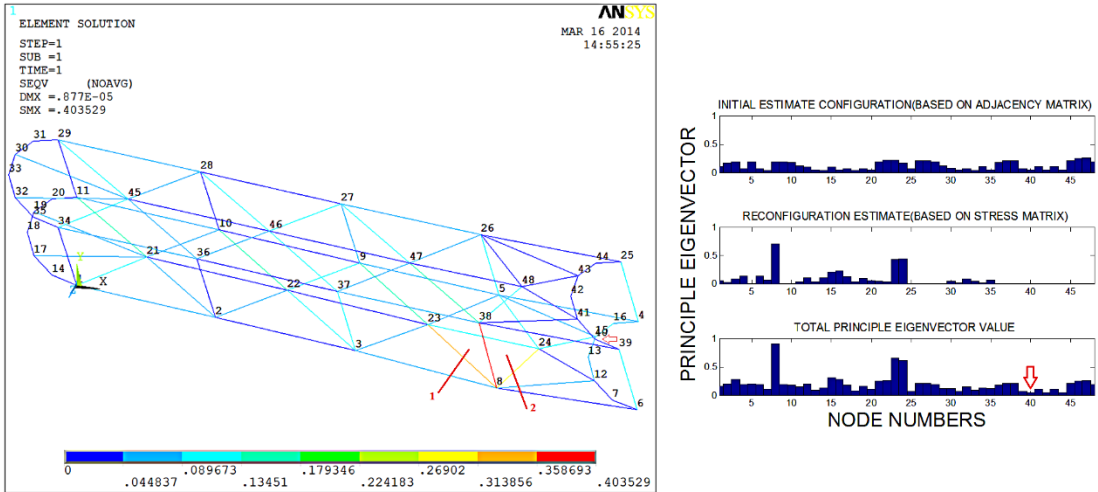


Figure 4.6: Initial Configuration Exoskeleton with Applying Force on Node 8

The loss of rigidity of the human limb together with the exoskeleton is then detected. This new force distribution overloading the exoskeleton is found by node sensors in hardware implementations. However, here, they are computed by Ansys. The link colors in Figure 4.6 reflect the stress distribution at the limits of the exoskeleton. The maximum stress value occurs at link between the 8<sup>th</sup> and 38<sup>th</sup> nodes in the whole structure, and takes the value 0.40MPA.

The stress analyses generate the need for a decision making towards reconfiguration which is carried out by first estimating the current configuration under this extra load using the graph theoretic method given in chapter 3. Our algorithm yields the new principle eigenvector components for nodes of the exoskeleton under excessive stress as shown in Figure 4.6. We notice that naturally the 8<sup>th</sup>, 23<sup>rd</sup> and 24<sup>th</sup> nodes under highest stress and they also have the expected maximum principle eigenvector components based on stress matrix, it should naturally not disconnect. To detect which robot disconnect, we must find the minimum principle eigenvector according the adjacency and stress matrix. The total principle eigenvectors obtained from adjacency and stress matrix is also shown in Figure 4.6. Accordingly, 8<sup>th</sup>, 23<sup>rd</sup>, and 24<sup>th</sup> nodes have the maximum principle eigenvector values; on the other hand, 40<sup>th</sup> node has the minimum one, being under less stress and neighbors. So it is labeled as idle node. The exoskeleton has to reconfigure so as to decrease the stress that the link between the 8<sup>th</sup> and 38<sup>th</sup> holons undergoes. The reconfiguration is now executed by disconnecting node that have minimum principle eigenvector component. This node than re-connects where the stress is highest and higher principle eigenvector, so as to provide extra support to the extra load condition, thus generating new configuration. Disconnecting the 40<sup>th</sup> node is decided due to its minimum principle eigenvector and since it has no other constraints, meaning total idleness. However, we have two areas to reconnect it to between 8<sup>th</sup> and 38<sup>th</sup>. First area is the between nodes 8, 23 and 38 and the second area is between nodes 8, 24 and 38. Total principle eigenvector value for node 23 is higher than the node 24, so we reconnect it to area 1.

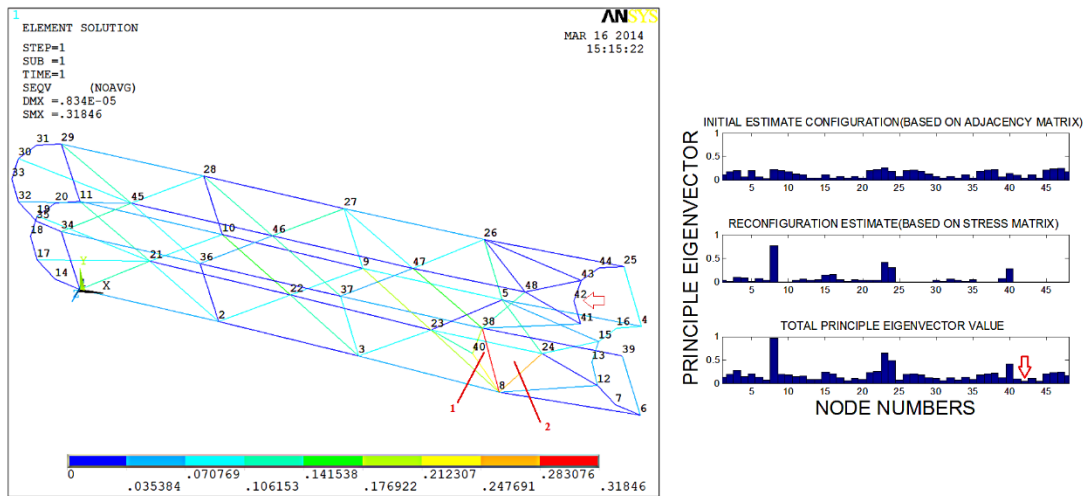


Figure 4.7: First Reconfigured Exoskeleton

Our new configuration of the exoskeleton and the new stress distribution of the reconfigured exoskeleton are given in Figure 4.7. The maximum stress that had occurred again on the link between 8<sup>th</sup> and 38<sup>th</sup> nodes dropped from 0.40MPa in the previous configuration of the exoskeleton. We relieved the excessive stress on this link however its not enough yet so, the system again undergoes the evaluation of the new principle eigenvector components to estimate the newly formed reconfiguration and determines the idle nodes in the current reconfigured exoskeleton structure.

For the first reconfiguration, the maximum principle eigenvector components based on the current estimation are 3<sup>rd</sup>, 5<sup>th</sup>, 8<sup>th</sup>, 9<sup>th</sup>, 10<sup>th</sup>, 21<sup>st</sup>, 22<sup>nd</sup>, 23<sup>rd</sup>, 24<sup>th</sup>, 26<sup>th</sup>, 27<sup>th</sup>, 28<sup>th</sup>, 36<sup>th</sup>, 37<sup>th</sup>, 38<sup>th</sup>, 45<sup>th</sup>, 46<sup>th</sup>, 47<sup>th</sup> and 48<sup>th</sup>, due to reconfiguration estimation 8<sup>th</sup>, 23<sup>rd</sup>, 24<sup>th</sup> and 40<sup>th</sup> nodes have the maximum ones as seen Figure 4.7. To make decision on which robot disconnect, the total principle eigenvector values are considered and the, 8<sup>th</sup>, 23<sup>rd</sup>, 24<sup>th</sup>, 38<sup>th</sup> and 40<sup>th</sup> nodes have maximum ones. We also know from Figure 4.7 that these nodes have higher stress link compared to those of other nodes. Note that 40<sup>th</sup> node which is disconnected robot previously, has a high principle eigenvector value for this new reconfiguration so it is seen as a critical holon.

In order to decrease further the stress in the newly reconfigured exoskeleton, a second reconfiguration step is generated by disconnecting the robot, which has minimum principle eigenvector, which is now the 42<sup>nd</sup> node. Again we have two areas to reconnect it; first area is nodes between 8, 38 and 40 and the second area is nodes between 8, 38 and 24 as shown in Figure 4.7 Because the principal eigenvector for node 24 is higher than the node 40, we reconnected it to second area and new configuration shown in Figure 4.8.

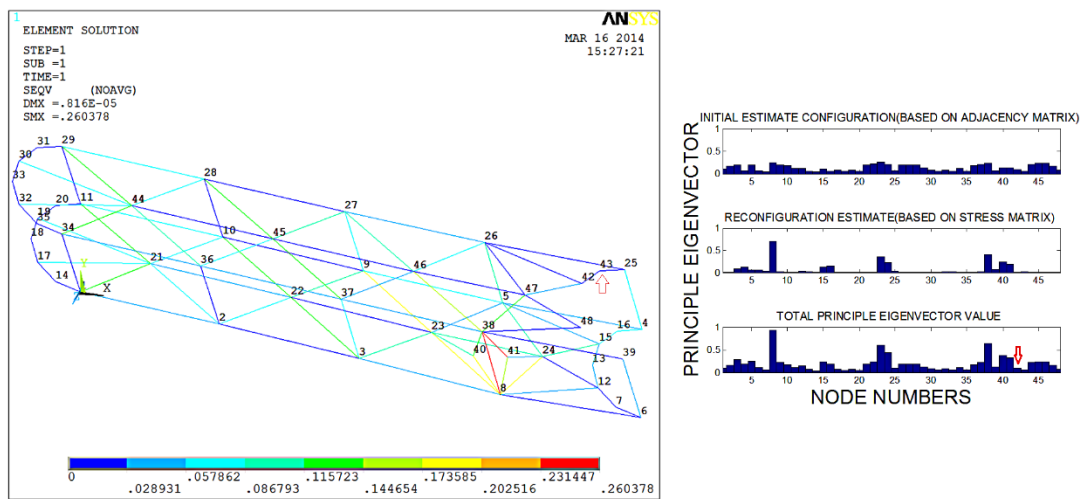


Figure 4.8: Second Reconfigured Exoskeleton

Consequently, the new exoskeleton configuration in this reconfiguration sequence is estimated and the maximum stress is found to occur in the link between the 38<sup>th</sup> and 41<sup>st</sup> with stress value 0.26 MPA. The link between 8<sup>th</sup> and 38<sup>th</sup> has now dropped from 0.31MPA in the previous configuration of the exoskeleton under extra load to that of 0.24 MPA in the current reconfigured exoskeleton, relieving the excessive stress on these two links.

At this new reconfiguration, the maximum principle eigenvector components based on the current estimation are 3<sup>rd</sup>, 5<sup>th</sup>, 8<sup>th</sup>, 9<sup>th</sup>, 10<sup>th</sup>, 21<sup>st</sup>, 22<sup>nd</sup>, 23<sup>rd</sup>, 24<sup>th</sup>, 26<sup>th</sup>, 27<sup>th</sup>, 28<sup>th</sup>, 36<sup>th</sup>, 37<sup>th</sup>, 38<sup>th</sup>, 45<sup>th</sup>, 46<sup>th</sup>, 47<sup>th</sup> and 48<sup>th</sup>, due to reconfiguration estimation 8<sup>th</sup>, 15<sup>th</sup>, 16<sup>th</sup>, 23<sup>rd</sup>, 24<sup>th</sup>, 38<sup>th</sup>, 40<sup>th</sup>, and 41<sup>st</sup> nodes have the maximum ones as seen Figure 4.8. To make decision on which robot disconnect, we consider the total principle eigenvector values. From these values, 8<sup>th</sup>, 23<sup>rd</sup>, 24<sup>th</sup>, 38<sup>th</sup>, 40<sup>th</sup>, and 41<sup>st</sup> nodes have maximum ones; while, nodes 14, 18, 20, 31, 33, 35 are the minimum ones; however these nodes are chosen as a fixed nodes so they cannot be disconnected. Therefore, we have to detect another idle node, which is 43<sup>rd</sup> node that has not any constrained. It reconnects to the node with highest stress and principle eigenvector and reconnected to highest stress link.

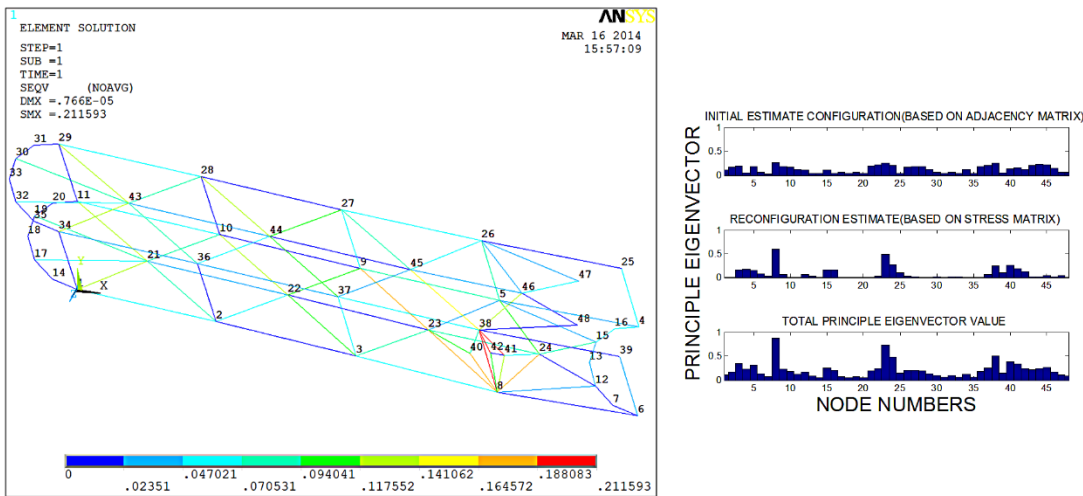


Figure 4.9: Final Reconfigured Exoskeleton

Finally, the new exoskeleton configuration in this reconfiguration sequence is estimated (Figure 4.9) and the maximum stress is found to occur in the link between

the 38<sup>th</sup> and 42<sup>h</sup> with stress value 0.21MPa which is the half of the maximum stress that obtained the initial configuration (Figure 4.6).

Our new exoskeleton is relieved of excess load and can carry more weights than the initial configuration. If we apply an extra -800N force to this final reconfiguration as shown in Figure 4.10, the magnitude of the maximum stress occur 0.40MPa which is nearly same with the initial configuration stress we reconfigured from Figure 4.6.

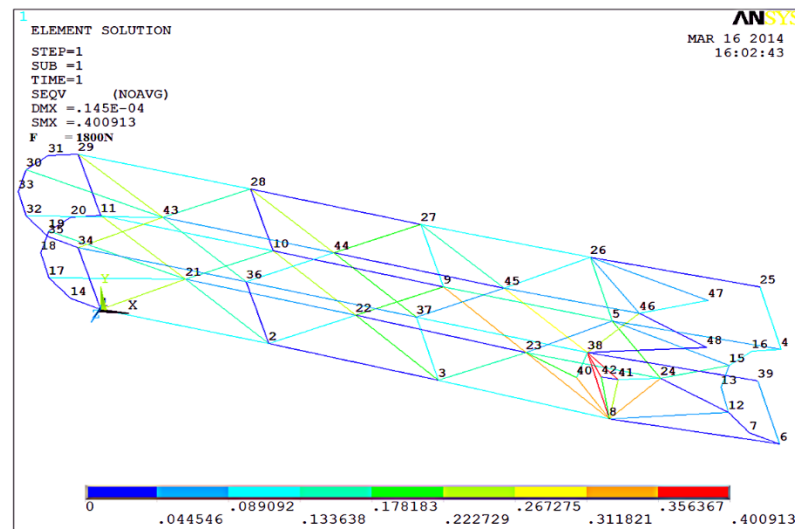


Figure 4.10: Final Reconfigured Stress Distributions with Extra load on Node 8

As a results, to decrease stress values to the below half of their individual maximum stress capacity, system undergoes reconfigurations sequences for three times. Nodes 40, 42, and 43 are selected as idle holons for initial, first, and second configurations respectively. After these nodes are reconnected, they have higher principle eigenvector values in the whole state as seen Table 4.2.

Table 4.2: Principle Eigenvector Values for Each Idle Node before and after Reconnection

Idle Nodes Numbers	Principle Eigenvector Values			
	Initial Configuration	First Configuration	Second Configuration	Final Configuration
40	0.04	0.37	0.37	0.39
42	0.05	0.04	0.31	0.34
43	0.06	0.05	0.06	0.25

### 4.3 Experiment 2: Reconfiguration Sequences with Applying Load on Two Nodes

In this part, our aim in this reconfiguration is again to hold all link stresses under half of this maximum stress capacity while applying 1000N forces at 2<sup>nd</sup> and 4<sup>th</sup> nodes towards to negative y- axis as shown in Figure 4.11 via the same fixed nodes introduced in the beginning of the chapter 4.

The principle eigenvector components of every holon based on estimation configuration (adjacency matrix) in the exoskeleton are presented in Figure 4.11. The maximum ones are seen to correspond to the 22<sup>nd</sup>, 23<sup>rd</sup>, 46<sup>th</sup> and 47<sup>th</sup> holonic robots. These are nodes having the most connections, and should be never disconnected. After applying extra loads at node 2 and 4, force distributions at each links and principle eigenvectors based on stress matrix are shown in Figure 4.11. According to these results, the link between the 4<sup>th</sup> and 25<sup>th</sup> is under the maximum stress (0.586).

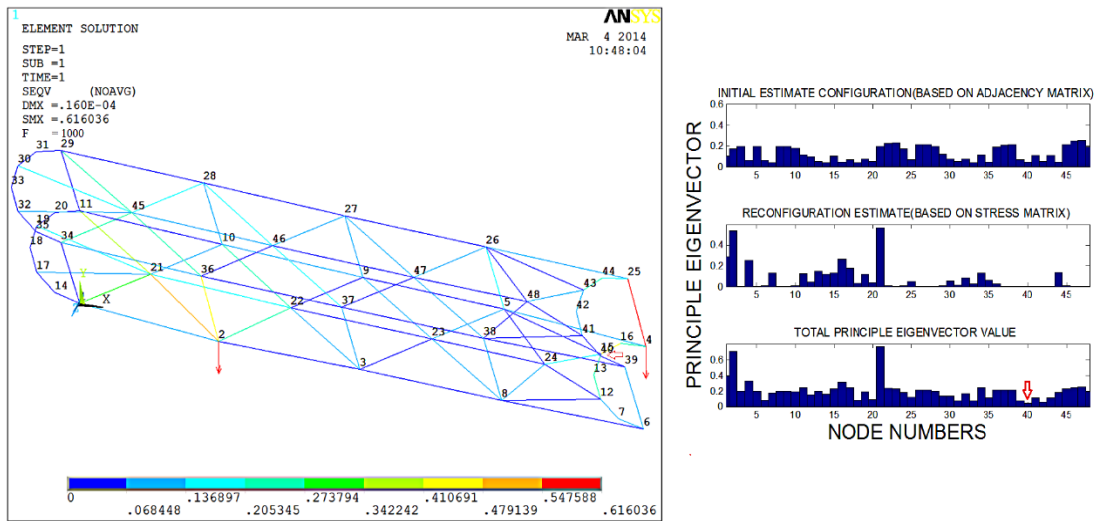


Figure 4.11: Initial Configuration Exoskeleton with Applying Force on Nodes 2 and

4

Note that, although we applied the same force at node 2 and node 4, the maximum stress occur around the node 4. Because, node 2 has more neighbors, so it can distribute the force to its neighbor easier than the node 4. To detect which robot will be disconnected for reconfiguration, we must find the minimum principle eigenvector according to the adjacency and stress matrix. According to the total principle eigenvectors shown in Figure 4.11, 1<sup>st</sup>, 2<sup>nd</sup>, 4<sup>th</sup>, 16<sup>th</sup> and 21<sup>st</sup> nodes have the maximum principle eigenvector values. On the other hand, 40<sup>th</sup> node has the minimum one, because it is under less stress and has fewer neighbors. So it is labeled as idle node.

The exoskeleton has to reconfigure in order to decrease stress at the link between the 4<sup>th</sup> and 25<sup>th</sup> holons. The reconfiguration is now executed by disconnecting the node 40<sup>th</sup> that have minimum principle eigenvector component, then reconnecting to the link between 4<sup>th</sup> and 25<sup>th</sup> nodes which has maximum stress and also to the 44<sup>th</sup> node,

because 44<sup>th</sup> node has higher principle eigenvector value than 41<sup>st</sup>, 42<sup>nd</sup> and 43<sup>rd</sup> nodes at this area.

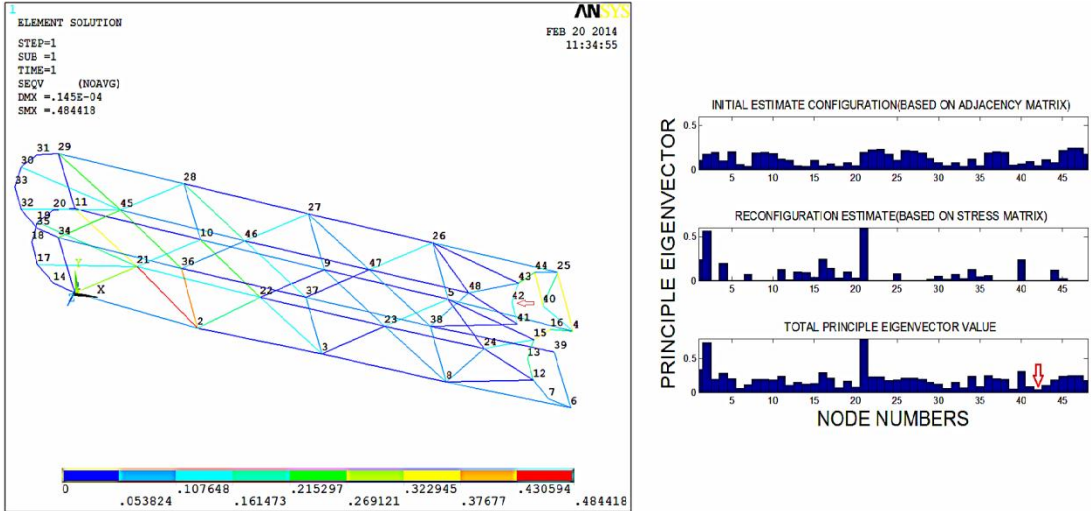


Figure 4.12: First Reconfigured Exoskeleton

The new configuration of the exoskeleton and the new stress distribution of the reconfigured exoskeleton are given in Figure 4.12. The maximum stress that had occurred on the link between 2<sup>nd</sup> and 21<sup>st</sup> nodes which is the node we applied force is 0.484MPa. The stress value of the link between 4<sup>th</sup> and 25<sup>th</sup> nodes in previous configuration was 0.58 MPa, but it decreased to 0.32 MPa in this configuration. So we have relaxed this link. The system again undergoes the evaluation of the new principle eigenvector components in order to estimate the newly formed reconfiguration, and determines the idle nodes in the current reconfigured exoskeleton structure.

At this new reconfiguration, the maximum principle eigenvector components based on the current estimation are 21<sup>st</sup>, 22<sup>nd</sup>, 26<sup>th</sup>, 45<sup>th</sup>, 46<sup>th</sup>, 47<sup>th</sup>, and due to the

reconfiguration estimation (stress matrix), 4<sup>th</sup>, 15<sup>th</sup>, 16<sup>th</sup>, 25<sup>th</sup>, 40<sup>th</sup> and 44<sup>th</sup> nodes have the maximum ones as shown in Figure 4.12. In order to make decision about which robot will be disconnect, we look at the total principle eigenvector values. Among these values, 1<sup>st</sup>, 2<sup>nd</sup>, 4<sup>th</sup>, 15<sup>th</sup>, 21<sup>st</sup>, and 40<sup>th</sup> nodes have maximum ones. We also know from Figure 4.12 that these nodes have higher stress link compared to those of other nodes. Note that 40<sup>th</sup> node was idle holon in previous configuration, but it became an important node in this new configuration. In order to decrease further the stress in the newly reconfigured exoskeleton, a second reconfiguration step is generated by disconnecting the robot which has minimum principle eigenvector, which is now the 42<sup>nd</sup> node and for this node there is no any constraint. It reconnects to the node where the stress is at highest. But, this node can be reconnect at two areas: first, the area of between nodes 1, 2 and 21, second, the area of 2, 21 and 22 as shown Figure4.12. However principle eigenvector for node 1 is higher than the node 22, so we reconnect this node at the first area. The second new reconfiguration is presented in Figure 4.13.

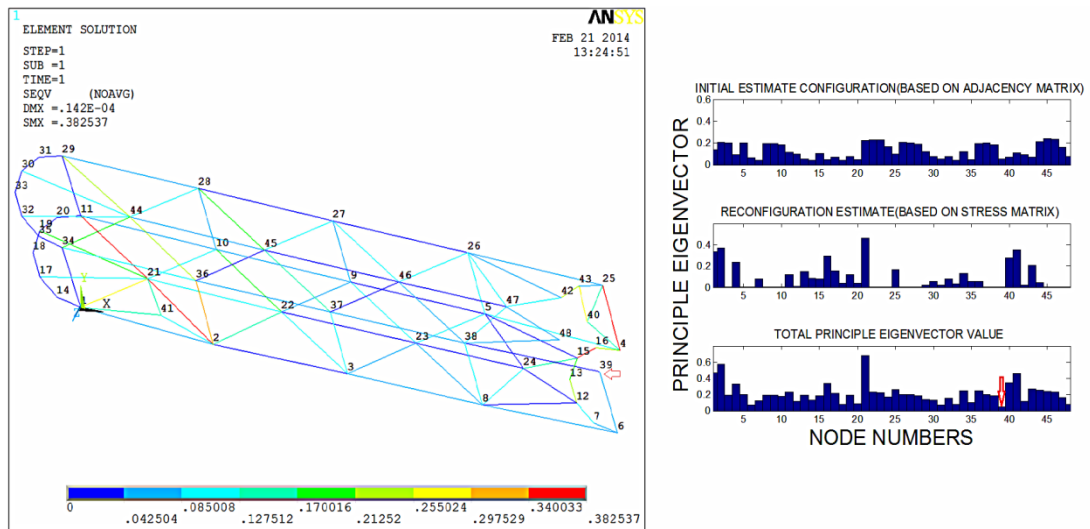


Figure 4.13: Second Reconfigured Exoskeleton

Our new exoskeleton configuration in this reconfiguration sequence is estimated, and the maximum stress is found to occur in the link between the 15<sup>th</sup> and 16<sup>th</sup> with stress value 0.38 MPA as seen Figure 4.13. The second higher stress (0.36 MPA) is obtained at the link between nodes 2 and 21 where we witness a further substantial decrease in link stress compared to the previous configuration which was 0.48 MPA. Be sure that node 42<sup>nd</sup> is selected as disconnected robot in previous reconfiguration and then reconnected as seen in Figure 4.13, but the name of that node became 41<sup>st</sup> node while it should be 42<sup>nd</sup> node. We mesh by using Ansys for all new reconfiguration, so Ansy can change mesh and node numbers.

At this new reconfiguration, the maximum principle eigenvector components based on the current estimation are 2<sup>nd</sup>, 5<sup>th</sup>, 9<sup>th</sup>, 10<sup>th</sup>, 21<sup>st</sup>, 22<sup>nd</sup>, 23<sup>rd</sup>, 36<sup>th</sup>, 37<sup>th</sup>, 38<sup>th</sup>, 45<sup>th</sup>, and 46<sup>th</sup>, and due to reconfiguration estimation (stress matrix), 1<sup>st</sup>, 2<sup>nd</sup>, 4<sup>th</sup>, 15<sup>th</sup>, 16<sup>th</sup>, 21<sup>st</sup>, 40<sup>th</sup>, 41<sup>st</sup>, and 43<sup>rd</sup> nodes have the maximum ones as seen Figure 4.13. In order to make decision about which robot will be disconnect, we look at the total principle eigenvector values. Among these values, 1<sup>st</sup>, 2<sup>nd</sup>, 4<sup>th</sup>, 16<sup>th</sup>, 21<sup>st</sup>, 40<sup>th</sup>, and 41<sup>st</sup> nodes have maximum ones; however, node 39 has the minimum principle eigenvector and there is no constraint, this node can be selected as an idle holon. So we disconnect it and then reconnect it between the link between the nodes 15 and 16 where there is the highest stress. New reconfiguration estimation is shown in the below Figure 4.14.

The new exoskeleton configuration in this reconfiguration sequence is estimated, and the stress is found to occur in the link between the 15<sup>th</sup> and 16<sup>th</sup> with stress value 0.26 MPA where we witness a further substantial decrease in link stress compared to the previous configuration which was 0.38 MPA. However, in this new configuration, the link between nodes 2 and 21 is under the maximum stress as seen Figure 4.14.

At this new reconfiguration, the maximum principle eigenvector components based on the current estimation are 2<sup>nd</sup>, 3<sup>rd</sup>, 5<sup>th</sup>, 8<sup>th</sup>, 9<sup>th</sup>, 10<sup>th</sup>, 21<sup>st</sup>, 22<sup>nd</sup>, 23<sup>rd</sup>, 26<sup>th</sup>, 27<sup>th</sup>, 36<sup>th</sup>

,37<sup>th</sup>, 44<sup>th</sup>, 45<sup>th</sup>, and 46<sup>th</sup>, and due to reconfiguration estimation (stress matrix), 1<sup>st</sup>, 2<sup>nd</sup>, 4<sup>th</sup>, 7<sup>th</sup>, 13<sup>rd</sup>, 15<sup>th</sup>, 16<sup>th</sup>, 21<sup>st</sup>, 25<sup>th</sup>, 39<sup>th</sup>, 40<sup>th</sup>, 41<sup>st</sup>, and 44<sup>th</sup> have the maximum ones as shown in Figure 4.14.

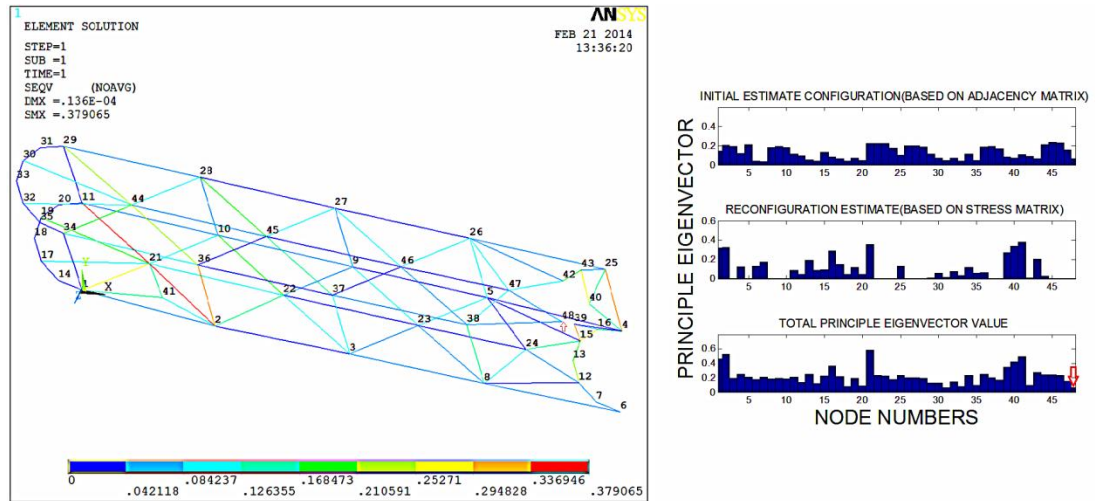


Figure 4.14: Third Reconfigured Exoskeleton

In order to make a decision about which robot disconnect, we look at the total principle eigenvector values. Among these values, node 31 has the minimum principle eigenvector; however it is selected as fixed node and should never be disconnected. So we must obtain the node which has the second minimum principal eigenvector. Node 48 has the minimum one and there is no constraint, so this node can be selected as an idle holon. Therefore we disconnect and then reconnect it at the link between the nodes 2 and 21. But we have two areas to reconnect; first, the area between the nodes 2, 21, and 22, and then the second area is between the nodes 2, 21 and 41. The principle eigenvector values for node 41 is higher than the node 22, so we reconnect it the second area as seen Figure 4.15.

Our new exoskeleton configuration in this reconfiguration sequence is estimated and the stress is found to occur in the link between the 2<sup>nd</sup> and 21<sup>st</sup> with stress value 0.26 MPA where we witness a further substantial decrease in link stress compared to the previous configuration which was 0.37 MPA. But in this new configuration, the link between nodes 11 and 21 has the maximum stress as seen Figure 4.15.

At this new reconfiguration as shown in Figure 4.15, the maximum principle eigenvector components based on the current estimation are 2<sup>nd</sup>, 3<sup>rd</sup>, 5<sup>th</sup>, 8<sup>th</sup>, 9<sup>th</sup>, 10<sup>th</sup>, 21<sup>st</sup>, 22<sup>nd</sup>, 23<sup>rd</sup>, 24<sup>th</sup>, 26<sup>th</sup>, 27<sup>th</sup>, 28<sup>th</sup>, 36<sup>th</sup>, 37<sup>th</sup>, 44<sup>th</sup>, 45<sup>th</sup>, and 46<sup>th</sup>, and due to reconfiguration estimation (stress matrix), 1<sup>st</sup>, 2<sup>nd</sup>, 6<sup>th</sup>, 7<sup>th</sup>, 13<sup>rd</sup>, 15<sup>th</sup>, 16<sup>th</sup>, 17<sup>th</sup>, 21<sup>st</sup>, 25<sup>th</sup>, 39<sup>th</sup>, 40<sup>th</sup>, and 41<sup>st</sup> nodes have the maximum ones.

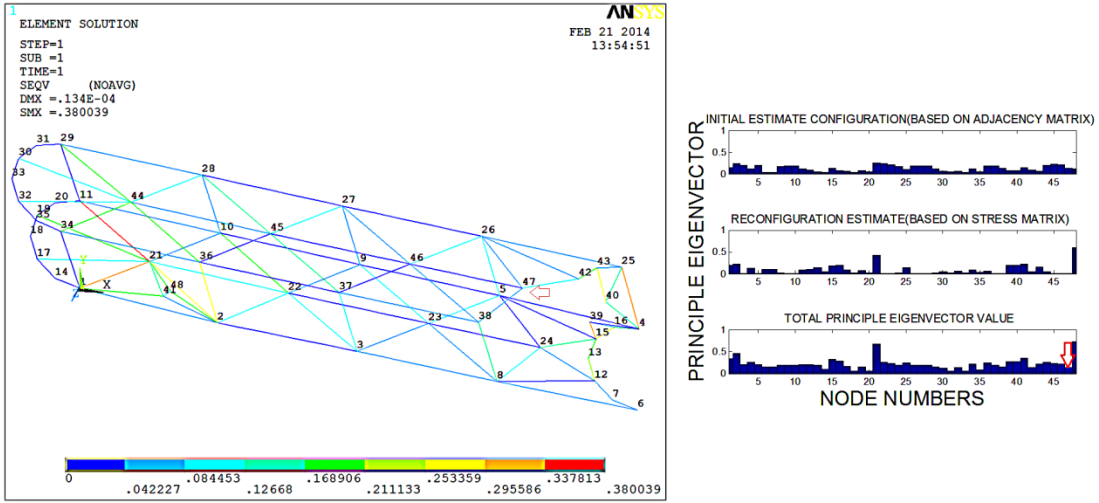


Figure 4.15: Fourth Reconfigured Exoskeleton

In order to make a decision about which robot disconnect to reduce stress again, we look at the total principle eigenvector values. Among these values, 14<sup>th</sup>, 18<sup>th</sup>, 20<sup>th</sup>, 31<sup>st</sup>, 33<sup>rd</sup> and 35<sup>th</sup> nodes have the minimum principle eigenvector values; however,

these nodes are selected as fixed nodes and should never be disconnected, so we must obtain the node, which has the minimum principal eigenvector. Node 47 has the minimum one, and there is no constraint. So this node can be selected as an idle holon. Therefore we disconnect and then reconnect it at the link between the nodes 11 and 21 as seen Figure 4.16.

Our new exoskeleton configuration in this reconfiguration sequence is estimated and the stress is found to occur in the link between the 11<sup>st</sup> and 21<sup>st</sup> with stress value 0.33 MPA(Figure 4.16) where we witness a further substantial decrease in link stress compared to the previous configuration which was 0.38 MPA (Figure 4.15).

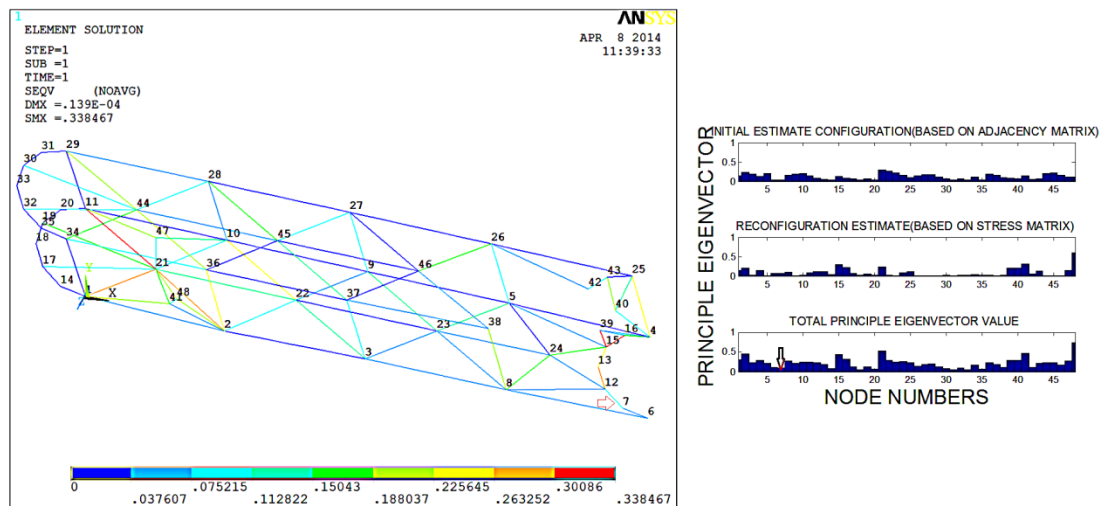


Figure 4.16: Fifth Reconfigured Exoskeleton

The system again undergoes the evaluation of the new principle eigenvector components in order to estimate the newly formed reconfiguration, and determines the idle nodes in the current reconfigured exoskeleton structure.

At this new reconfiguration as shown in Figure 4.16, the maximum principle eigenvector components based on the current estimation are 2<sup>nd</sup>, 3<sup>rd</sup>, 5<sup>th</sup>, 8<sup>th</sup>, 9<sup>th</sup>, 10<sup>th</sup>, 11<sup>st</sup>, 21<sup>st</sup>, 22<sup>nd</sup>, 23<sup>rd</sup>, 24<sup>th</sup>, 26<sup>th</sup>, 27<sup>th</sup>, 28<sup>th</sup>, 36<sup>th</sup>, 37<sup>th</sup>, 43<sup>rd</sup>, 44<sup>th</sup>, and 45<sup>th</sup>, and due to reconfiguration estimation (stress matrix) 1<sup>st</sup>, 2<sup>nd</sup>, 15<sup>th</sup>, 16<sup>th</sup>, 21<sup>st</sup>, 39<sup>th</sup>, 41<sup>st</sup>, 42<sup>nd</sup> and 47<sup>th</sup> have the maximum ones. In order to make a decision about which robot disconnect, we look at the total principle eigenvector values. From these values, 2<sup>nd</sup>, 15<sup>th</sup>, 16<sup>th</sup>, 21<sup>st</sup>, 39<sup>th</sup>, 41<sup>st</sup>, 42<sup>nd</sup>, 44<sup>th</sup>, and 47<sup>th</sup> nodes have maximum ones. In order to further decrease the stress in the newly reconfigured exoskeleton, a new reconfiguration step is generated by disconnecting the robot, which has minimum principle eigenvector, which is now the seventh node, and there is no constraint for this node. Therefore, we disconnect and then reconnect it at the link between the nodes 11, 21 and 47 as seen Figure 4.16.

The new configuration of the exoskeleton and the new stress distribution of the reconfigured exoskeleton are presented in Figure 4.17. The maximum stress that had occurred on the link between 15<sup>th</sup> and 39<sup>th</sup> nodes where we applied force is 0.33MPA, and the link between 11<sup>st</sup> and 21<sup>st</sup> nodes has now dropped from 0.27 MPA to 0.33 MPA in this new configuration. So we have relaxed the link. The system again undergoes the evaluation of the new principle eigenvector components in order to estimate the newly formed reconfiguration, and determines the idle nodes in the current reconfigured exoskeleton structure. For this structure node 9 selected as an idle holon so, we disconnect and then reconnect it at the link between the nodes 15, 16 and 39 as seen Figure 4.18.

Finally, the new configuration of the exoskeleton and the new stress distribution of the reconfigured exoskeleton are given in Figure 4.18. The maximum stress is half of the initial maximum stress as seen Figure 4.11.

Thus our new exoskeleton is relieved of excess load, and can carry more weights than the initial configuration (Figure 4.11). If we apply an extra -900N force to this

final reconfiguration as shown in Figure 4.19, the magnitude of the maximum stress occur 0.60MPa which is almost same with the initial configuration stress we reconfigured from Figure 4.11.

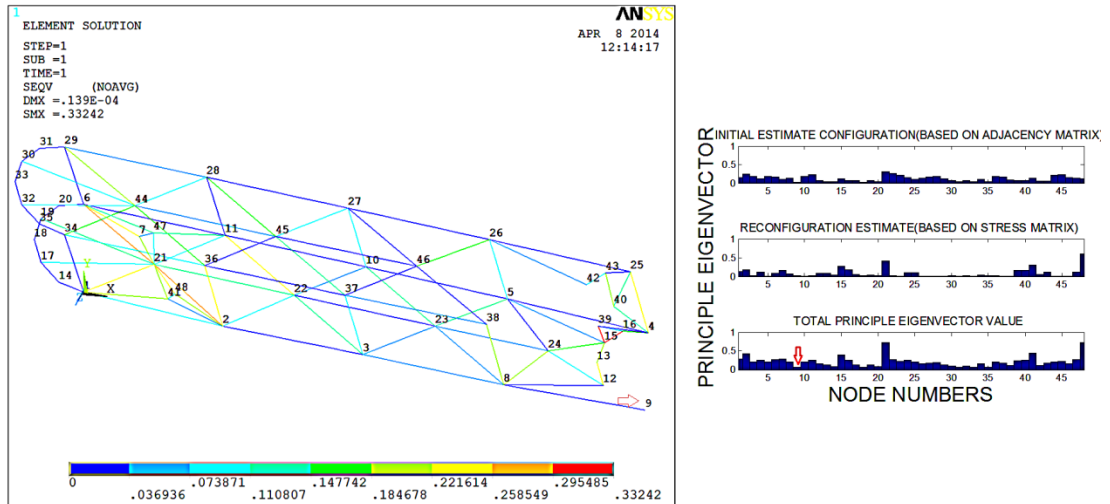


Figure 4.17: Sixth Reconfigured Exoskeleton

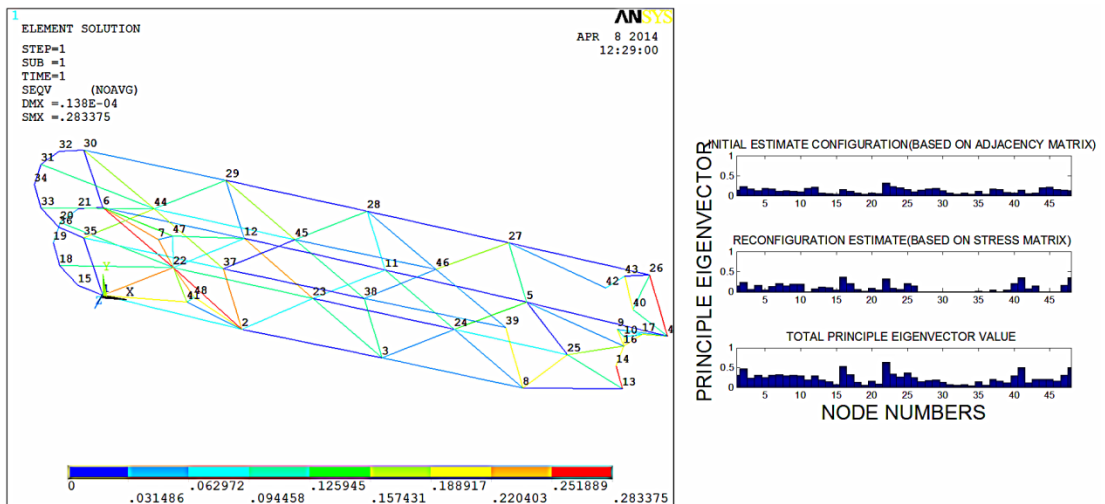


Figure 4.18: Final Reconfigured Exoskeleton

Until now, we reduce the stress by half of the initial configuration while applying forces on nodes 2 and 4. How can our state change when applying an extra load during the decision making? As we mentioned before at the algorithm procedure at the section 3.3. If there is any extra load obtained after reconfiguration estimate, the system continues with the decision-making procedure, but if any new load is detected, then the system comes back to reconfiguration estimate. Let us think Figure 4.13, if system does not detect any external force, node 39 will be selected as a idle holon. But during the decision making procedure we applied 300N force on node 39, so system have to return the reconfiguration estimation to detect new idle holon. According the new stress distributions as seen Figure 4.20, node 48 is selected as new idle holon.

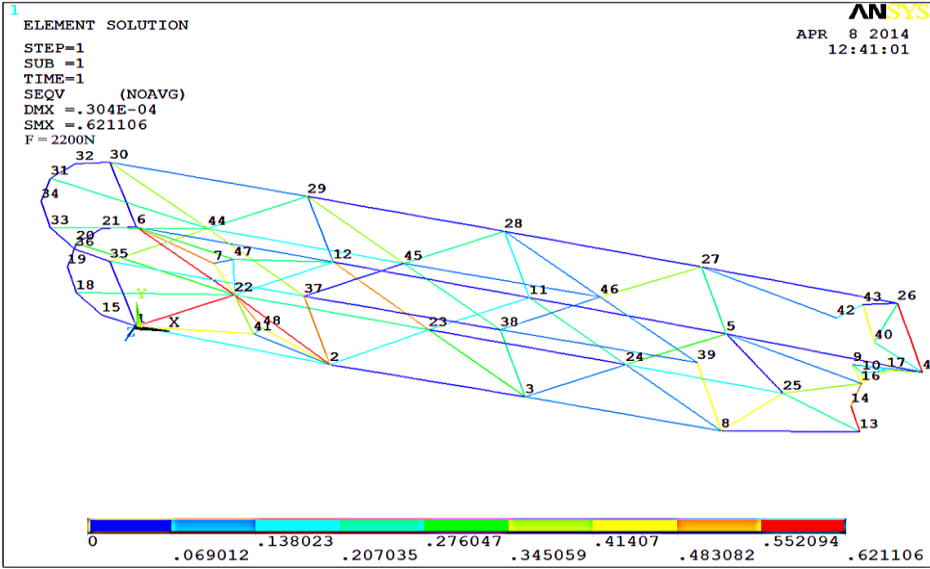


Figure 4.19: Final Reconfigured Stress Distributions with Extra load on Nodes 2 and

As a results, to decrease stress values to the below half of their individual maximum stress capacity in this experiment, system undergoes reconfigurations sequences for seven times. Nodes 40, 42, 39, 48, 47, 7, and 9 are selected as idle holons for each configuration respectively. After these nodes are reconnected, they have higher principle eigenvector values in the whole state as seen Table 4.3.

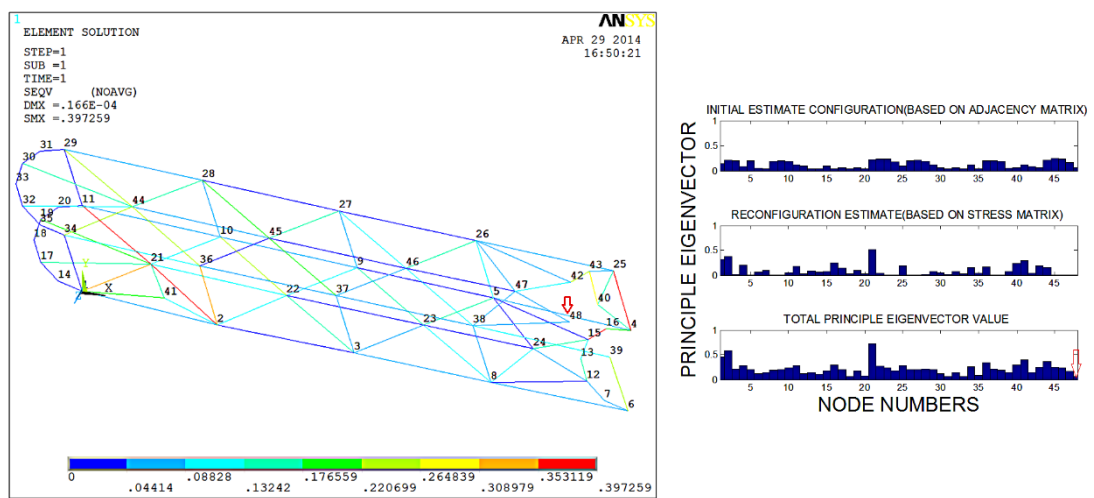


Figure 4.20: Reconfigured Stress Distributions with Applying Load on Nodes 2, 4, and 39

Table 4.3: Principle Eigenvector Values for Each Idle Node before and after Reconnection

Idle Nodes Numbers	Principle Eigenvector Values							
	Initial Config.	First Config.	Second Config.	Third Config.	Fourth Config.	Fifth Config.	Sixth Config.	Seventh Config.
40	0.04	0.31	0.34	0.41	0.41	0.41	0.41	0.41
42	0.05	0.04	0.46	0.49	0.49	0.49	0.49	0.49
39	0.07	0.05	0.05	0.34	0.33	0.33	0.33	0.33
48	0.18	0.17	0.07	0.06	0.83	0.80	0.80	0.80
47	0.15	0.13	0.09	0.08	0.08	0.35	0.35	0.35
7	0.16	0.11	0.11	0.20	0.15	0.08	0.32	0.32
9	0.2	0.19	0.19	0.19	0.18	0.1	0.07	0.31

#### 4.4 Sensitivity Analysis

In these thesis we have four main questions that we can discuss.

1. How do stress distributions change on each link while increasing the applying forces?
2. What kind of things will change at our structure when increase the mesh numbers?
3. How can stress distributions change at new reconfiguration while we connect the nodes other areas?
4. If we add the values of the nodes, how does the system's stress distribution change?

All these questions will be answered in this part.

#### 4.4.1 Relationship between Force and Stress

As we mentioned before, stress can define as a force per unit area (Force/Area). So, increasing forces resulted with a higher stress at each link. Let's think the Figure 4.6 which we applied -1000N force on the node 8 and maximum stress (0.40MPa) occur at the link between nodes 6 and 39. However, if we apply -500N on the same node, the maximum stress is obtained at the same link as seen Figure 4.21 which is the half of the initial force as shown Figure 4.6. Also stress distributions of each node for both cases is determined and given in Figure 4.21. From these values if we apply doubled force, stress distributions at each node also doubled.

From the Figure 4.21, we select special element, which is the link between nodes 8 and 38. The stress distribution changing based on different force values are determined and shown in the Figure 4.22. According to this figure, stress value increase continually with increasing force value.

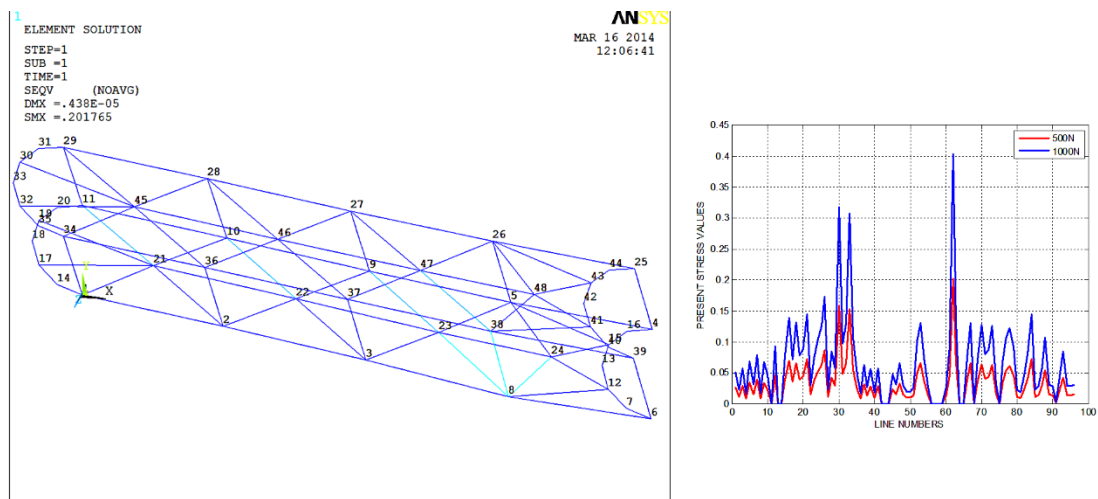


Figure 4.21: Stress Values of each Node with Different Forces Magnitudes

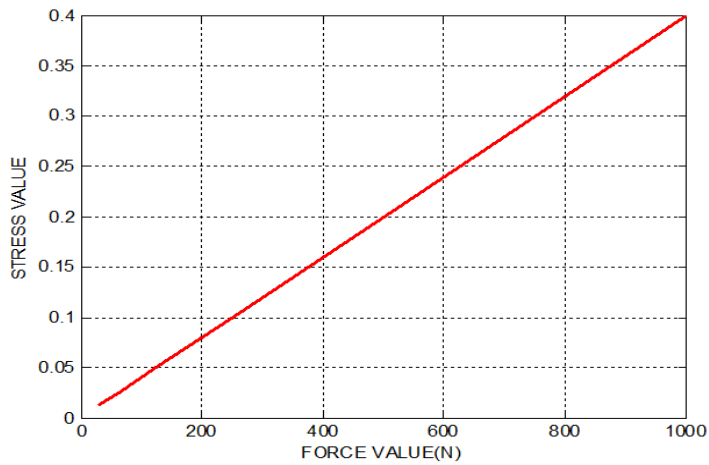


Figure 4.22: Stresses-Forces Diagram

#### 4.4.2 Reconnection Criteria

In our procedure, after obtaining the idle holons, which will be disconnected, we reconnect it to between three nodes; two nodes belong to highest stress link and one node belongs to the higher principle eigenvector at this area. In the 2<sup>nd</sup> Experiment simulation part as seen Figure 4.11, node 40 is selected as idle holon so it is disconnected and it is reconnected the highest stress link between the node 4 and 25. Also in this area we have nodes 41, 42, 43, and 44 and we also reconnect the idle holon to node 44 which has the higher principle eigenvalue in this area. So we can decrease stress at the link between node 4 and 25 to 0.37MPa from 0.57MPa as shown Figure 4.11.

But if we reconnect the idle holon to other nodes, what will change? If we reconnect node 40 only to link between nodes 4 and 25, stress distributions are like in Figure 4 23.

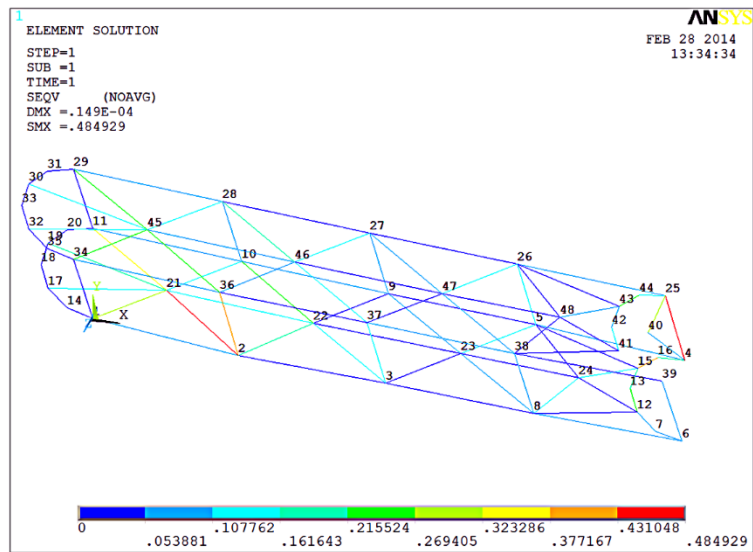


Figure 4.23: Reconnection to Only Two Nodes

As seen Figure 4.23, the maximum stress (0.484MPa) again occur at the link between nodes 4 and 25. So for this configuration we have to find an idle holon to again reduce the stress at the same link. After that we can decrease the stress at the link between nodes 2 and 21. However, For the figure 4.11, the maximum stress is obtained the link between nodes 2 an 21. Therefore, this connection gives us an additional iterative so it is not convenient.

Another situation is reconnecting the node 40 to other nodes on the highest stress area. At Figure 4.11, we reconnect it to node 44, which is higher principle eigenvalues than nodes 41, 42, and 43. If we reconnect it to node 43, stress distribution is like in Figure 4.24. From this figure we reduce the stress (0.39) at the link between the nodes 4 and 25; however the link between nodes 40 and 43 has the highest stress (0.48) on the configuration so for the next step we must decrease the stress at this link. After that we can decrease the stress at the link between nodes 2 and 21. This gives me an additional iterative so it is not convenient.

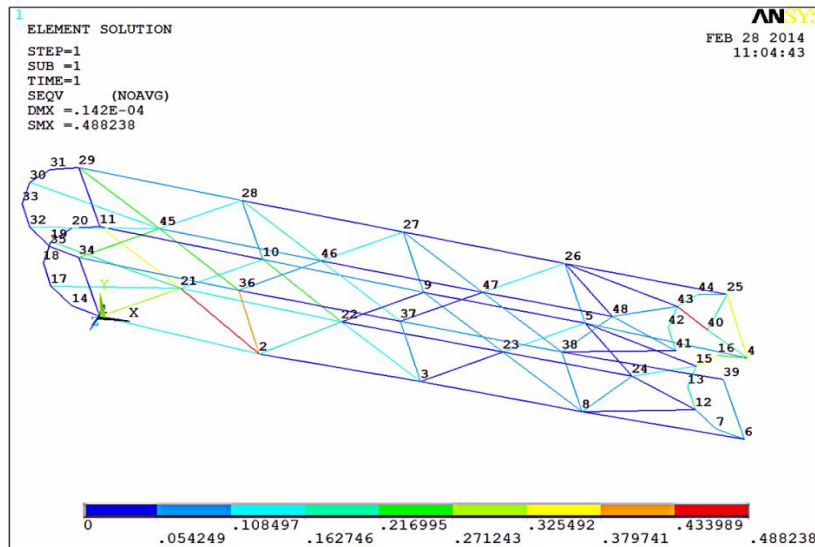


Figure 4.24: Reconnection to Other Node at the Same Area

If we reconnect it to more than three nodes, stress distribution is like in Figure 4 25.

In this configuration as shown Figure 4.25, the maximum stress is obtained at the link between the nodes 2 and 21. Also the stress value at the link between node 4 and 25 decreases to 0.35MPa from the 0.57 MPA. From these results, more connection seems to reduce stress at this link, but the stress at the link between nodes 40 and 42 occur 0.39MPa which is more than Figure 4.11. The other disadvantage is that these more connections result with higher principle eigenvector values for these nodes. Therefore, in the whole structure, it can cause to find less idle holons for new reconfiguration, so it is not convenient.

So from these aspects, connecting three nodes is more convenient than other situations.

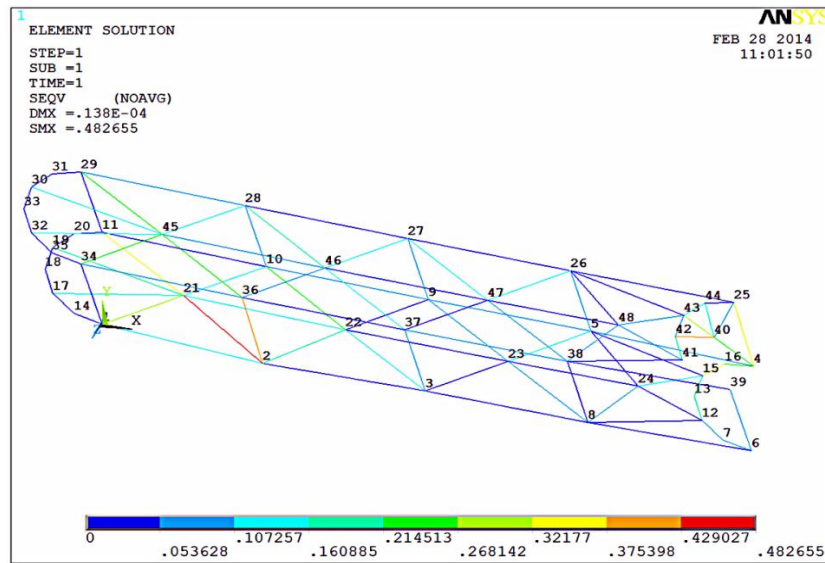


Figure 4.25: Reconnection to More Than Three Nodes

#### 4.4.3 Increasing Mesh Numbers

For the initial configuration (Figure 4.6), we have totally 48 nodes and 92 links. In the new configuration as seen Figure 4.26 below, we have totally 61 nodes and 141 links and, in this part, we compare the difference and similarities from the initial configuration as shown in Figure 4.2

For Figures 4.6 and 4.26, we applied to -1000N force at the same place. For the initial configuration (Figure 4.6) stress value at the link between nodes 8 and 38 is 0.40MPa; however, for the new configuration (Figure 4.26), this value drop to 0.34, because node 8 has six neighbors for initial configuration and has 8 neighbors for this configuration. Therefore the advantage of increasing mesh number is reliving the less stresses on the links.

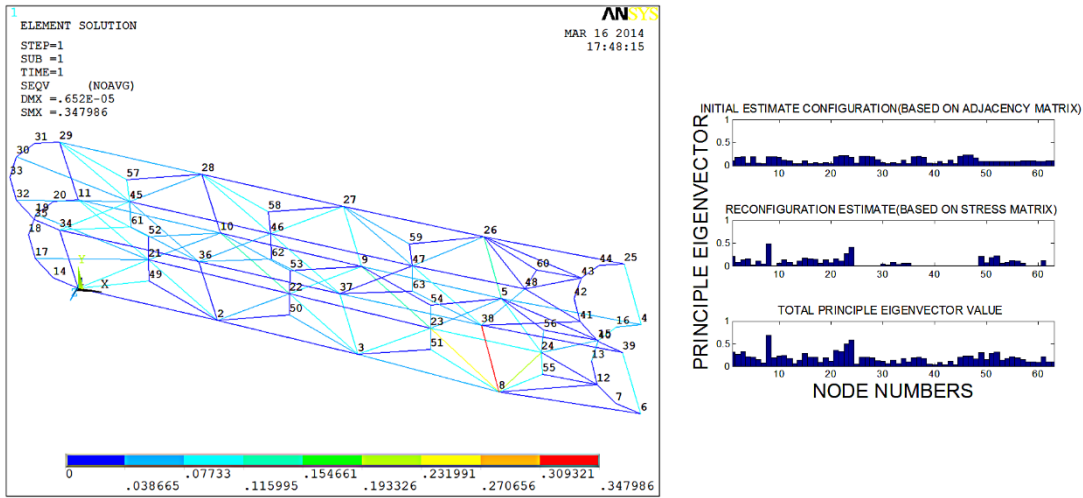


Figure 4.26: Exoskeleton with Increasing Mesh Numbers

For the new configuration as seen Figure 4.26, the average total principle eigenvector values for each node is 0.17 and principle eigenvector values of approximately 34 nodes are under this average value; however, the average total principle eigenvector values for each node at initial configuration (Figure 4.6) is 0.20 and 18 nodes are under the average. Its mean that for the Figure 4.26, we have nearly 34 idle holons; however, for the initial configuration (Figure 4.6) we have 18 idle holons. Therefore, increase of mesh number gives us advantage to select more idle holons during the reconfiguration and also help us further decreasing stresses between the links.

Disadvantage of increasing mesh is the delay of decision making process. For the initial configuration, it takes 10 seconds to obtain idle holon; however, for the new configuration (Figure 4. 26) it takes nearly 18 seconds.

#### 4.4.4 Stress Distributions with Including the Mass of Nodes

As seen in Figure 4.13, if the weights of the nodes are neglected, the maximum stress within the system (0.38MPa) is measured between the node 15 and node 16.

If the weights of the nodes within the system are taken into the account and the weight of each of nodes is taken as 1 kg, the new stress distribution is as seen in Figure 4.27. According to this figure, the maximum stress has been measured between 1<sup>st</sup> node and 21<sup>st</sup> node, and its value is 0.50MPa. Since the nodes at shoulder region are kept fixed during the analyses, the highest effect of the gravity is observed at this point. And this situation led the stress value to increase from 0.38MPa to 0.50MPa. That's why; the next move of the node will be to decrease the stress between 1<sup>st</sup> node and 21<sup>st</sup> node. If the weights of the nodes were neglected, it would try to decrease the stress on the link between 15<sup>th</sup> node and 16<sup>th</sup> node.

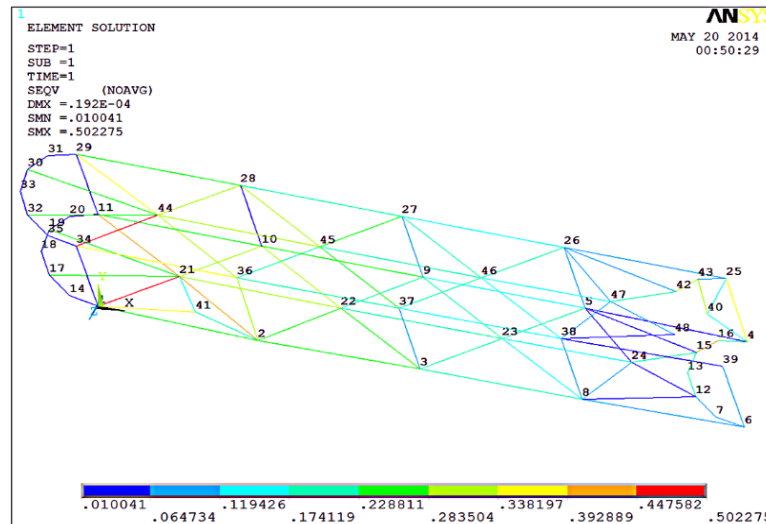


Figure 4.27: Stress Distributions with Including Mass of Nodes



## CHAPTER 5

### HARDWARE IMPLEMENTATION

The novelty of this thesis lies behind designing exoskeleton structure by using self-reconfigurable modular robots. However, these modular robots have not been sold yet, even if it is possible, we cannot design such an exoskeleton because of their size. So for testing the algorithm on the hardware application, we use bioloid robotic kits to design our exoskeleton structure to proof our concept. These robots kits are not capable of communication with neighbors, disconnecting or reconnecting. Therefore it is not possible to test our algorithm given in chapter 3 on this robots kits. We compare the producing torque values of each module to detect disconnected module in the structure.

Properties of each module utilized in experiment are given in Table 5.1.

Table 5.1: Properties of Modules

Weight	54.6 gr
Initial Position	150°
Moving Speed	3.33 RPM
Maximum Torque	1.5N.m

Each module can lift up to 330gr so it is impossible for us to test the exoskeleton structure on the actual adult human arm. The other problem is that we do not reconnect them like self-reconfigurable robots. Therefore, we just only test structure rotating only the elbow part with applying fewer forces on other modules.

### 5.1 Experiment 1: Exoskeleton Structure with 10 Nodes

In this part, we design a exoskeleton structure such that contains 10 modules and each module is connected consecutively like as a human arm shape as shown in 'Figure 5.1, and the module 3 and 4 are thought as an elbow joint. The total weight of the system is 600 gr.



Figure 5.1: Current Exoskeleton Structure

In this implementation, our expectation is the 3<sup>rd</sup> and 4<sup>th</sup> module bending the robot arm nearly 30° along the y-axis while applying forces on modules 5, 6, 7, 8, 9, and 10

to come to  $120^\circ$  from  $150^\circ$ , while other servo motors positions are kept constant during the experiment. Initially, we applied 400gr load on the motors, and we test the structure whether it can bend the robot arm with forces or do not.



Figure 5.2: Exoskeleton with 400gr load

As seen Figure 5.2, modules 3 and 4 can bend the arm  $30^\circ$  with using half of their maximum torque capacities.

Then we test the structure while increasing load values to 1kg as seen Figure 5.3 and we test the structure whether it can bend the robot arm with forces or do not.

For this situation, module 3 and 4 cannot bend the arm as shown in Figure 5.3. Therefore, system has to undergo reconfiguration sequence to twist elbow part of the exoskeleton by detecting idle modules automatically. Present torque values of each module is considered in order to make a decision about which module is disconnected and where it is reconnected again to lift loads and also to reach goal position.

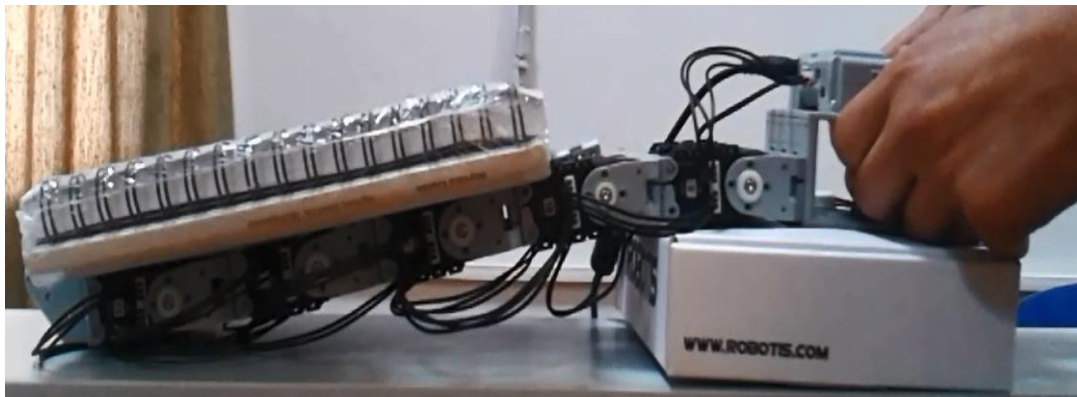


Figure 5.3: Exoskeleton with 1kg load

According to the present torque values of each module as shown in Figure 5.4, modules 3 and 4 reach the maximum torque capacities (1.5 N), while modules 9 and 10 produce minimum torques (0) during the experiment. So, the system can choose modules 9 and 10 as idle nodes as shown in Figure 5.5. In this experiment, we disconnected node 9 and reconnected it again between nodes 3 and 4 that have produced maximum torques.

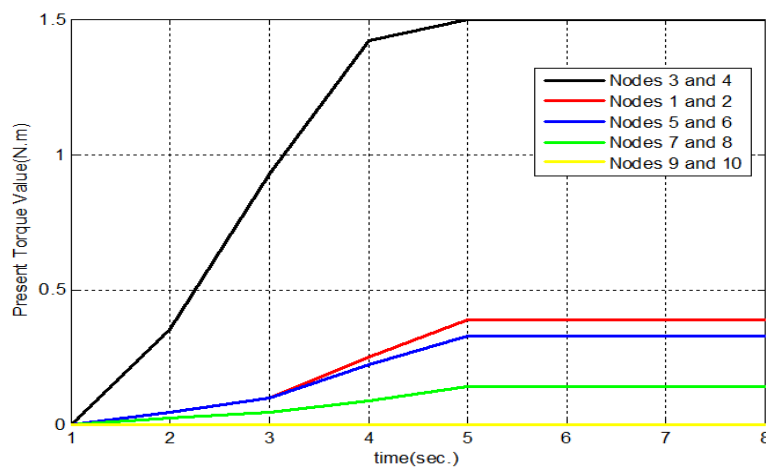


Figure 5.4: Present Torque Values of Each Module



Figure 5.5: Selecting Disconnected Module

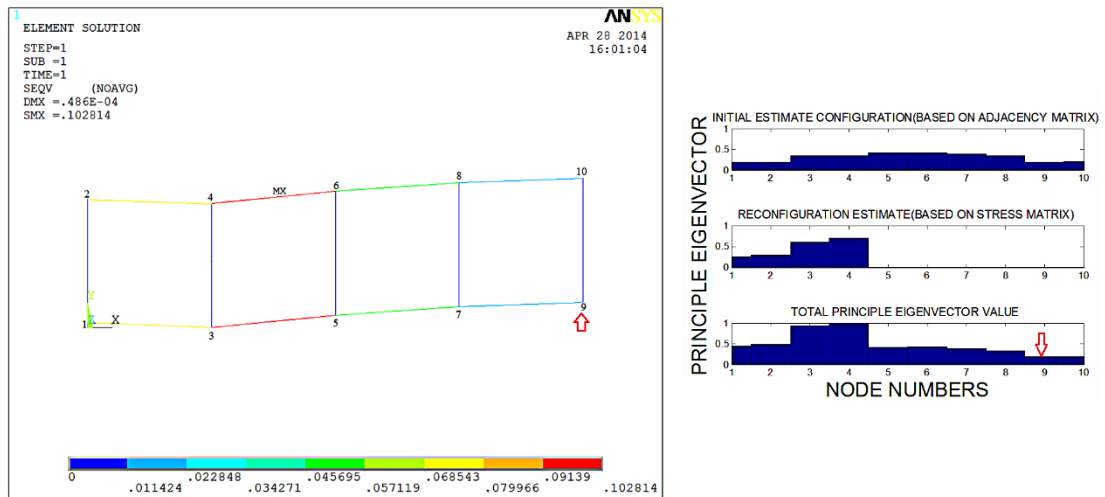


Figure 5.6: ANSYS Analysis of Exoskeleton Structure

Figure 5.6 shows the simulation of hardware applications and principle eigenvector values of each module being under load. Modules 3 and 4 are exposed to maximum load and it has maximum principle eigenvector, whereas modules 9 and 10 has the less load and minimum principle eigenvector. So node 9 is selected as an idle robot and chosen as a disconnected robot and reconnect to near the nodes 3 and 4.

Finally, after we reconnect the module 9, we obtain the new structure as seen Figure 4.27. At new structure, modules 3,4 and 9 are thought as elbow joints and these modules bend the arm together.



Figure 5.7: Reconfigured Exoskeleton Structure

Now, we test the new structure whether it can bend the robot arm with 1kg forces or do not.

Results obtained from Figure 5.8 shows that new structure is capable of bending the arm.

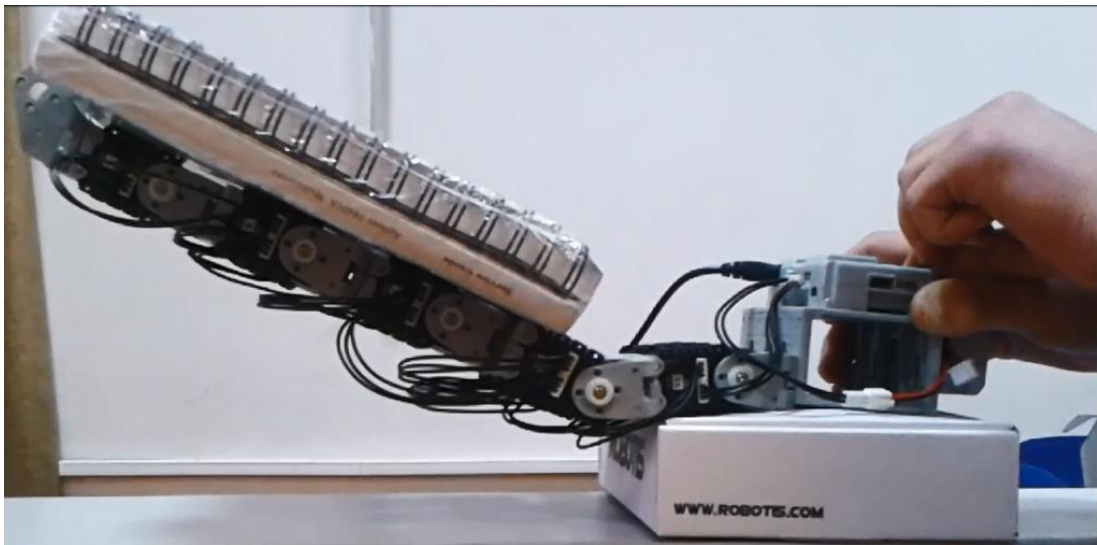


Figure 5.8: Reconfigured Exoskeleton with 400gr load

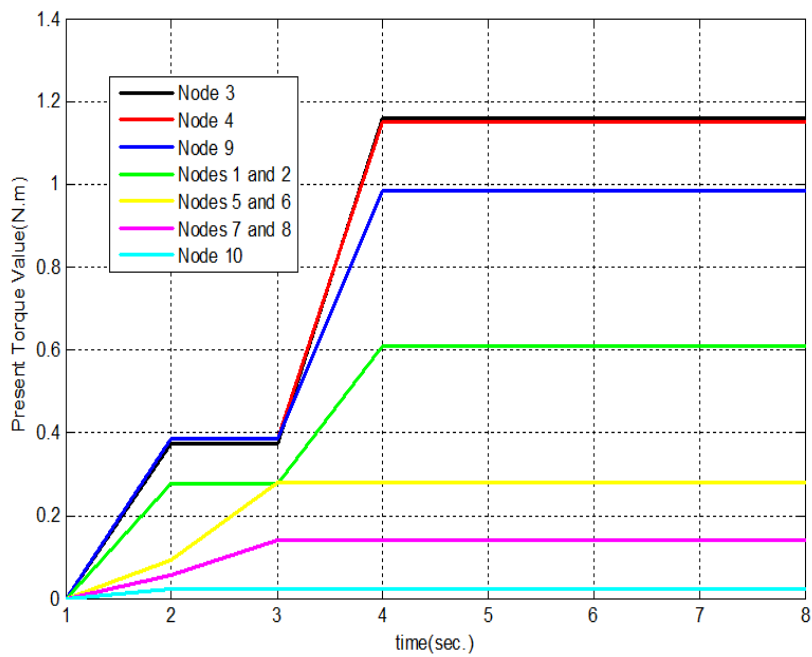


Figure 5.9: Present Torque Values of Each Module at Reconfigured Exoskeleton

During experiment modules 3, 4, and 9 produce torques which are less than the maximum torques capacities to come to target position (120°) as seen Figure 5.9.

The simulation of current exoskeleton structure is given in Figure 5.10, and the maximum stress is 0.076MPa dropped from 0.1MPa (Figure 5.6).

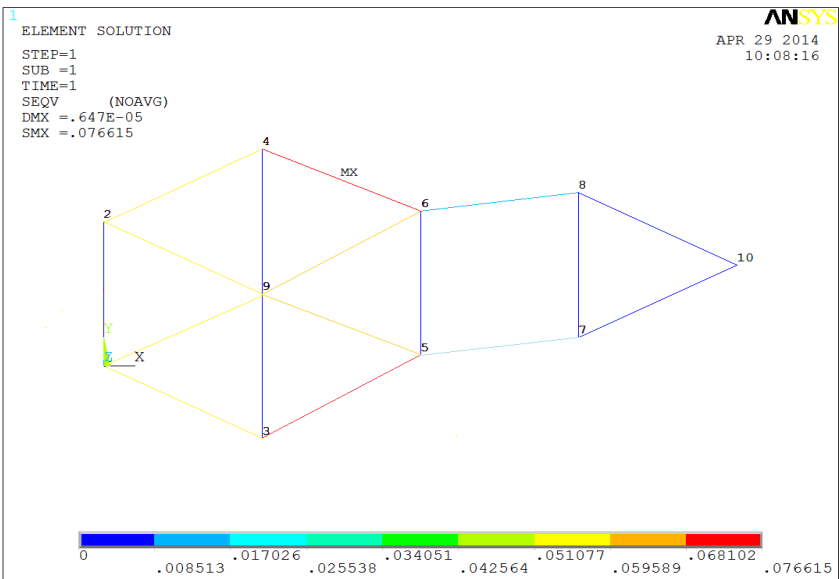


Figure 5.10: ANSYS Analysis of Exoskeleton Structure

### 5.2 Experiment 2: Exoskeleton Structure Supporting Arm

In this experiment our procedure is:

The arm, initially, tries to lift the weight while exoskeleton is offline. When the arm cannot lift the weight, the exoskeleton becomes a part of activity, so the weight is

lifted by both arm and exoskeleton. If the system still cannot lift the weight, the exoskeleton reconfigures the system in order to lift the weight.

In this part, our system consists of two parts. First part (upper part) consists of modules 1, 2 and 3 and a wooden part as seen Figure 5.11. This part is considered to be the human arm, and modules represent the elbow part, while the wooden part represents the link. Second part (bottom part) as shown in Figure 5.12 is the exoskeleton consisting of modules 4, 5,6,7,8,9,10, and 11. The exoskeleton supports the arm by being adhered to bottom. The weight of our arm is 300g, and the weight of exoskeleton 450 g, and total weight of the system is 750g.

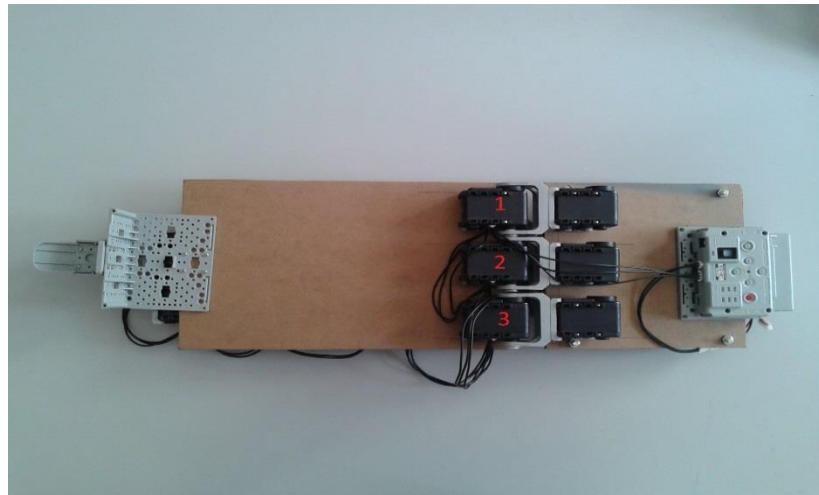


Figure 5.11: Upper Part of Our System (Arm Part)



Figure 5.12: Bottom Part of Our System (Exoskeleton Part)

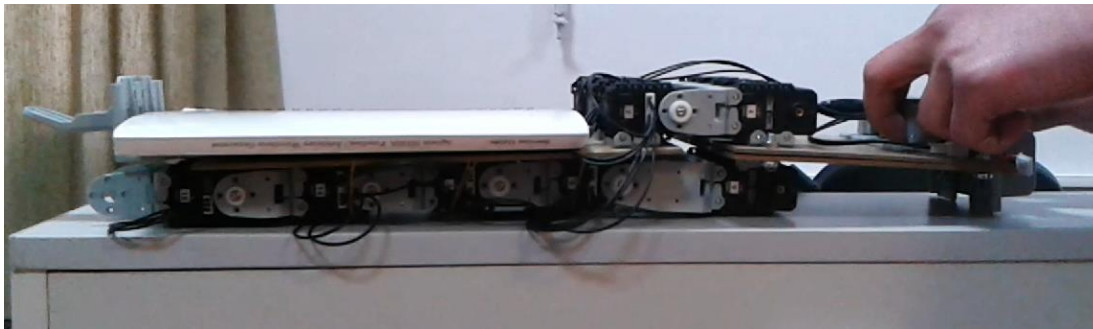


Figure 5.13: Applying 300 g load on Arm

Initially, as seen in Figure 5.13, 300g of weight load is applied on arm. In this case, there is the load of this 300 g and the weight of exoskeletons' own loaded on arm, so the total load on arm is 750g. It is being assessed if only the arm can lift this weight or not.

As seen in Figure 5.14, the arm can lift the loaded weight without the support of exoskeleton. During the operation, modules 1, 2 and 3 produce 0.78N.m, 0.73N.m and 0.62MPA respectively which are less than their maximum torque capacities.

Then, as seen in Figure 5.15, we increased the weight loaded on arm from 300g to 1kg, and it was evaluated if the arm can lift this weight by itself or not.

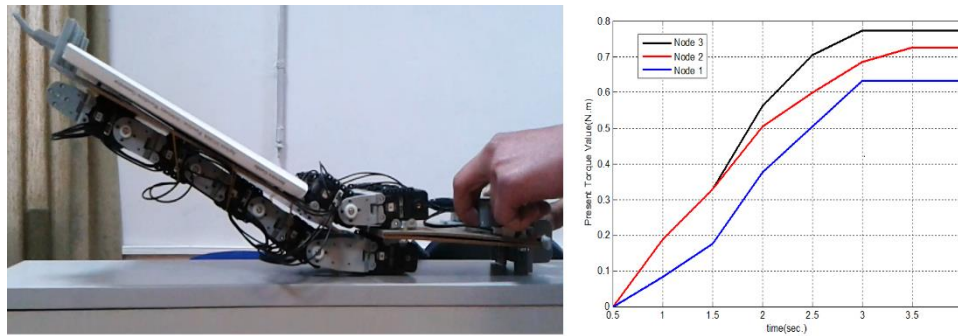


Figure 5.14: Present Torque Values on Arm Modules

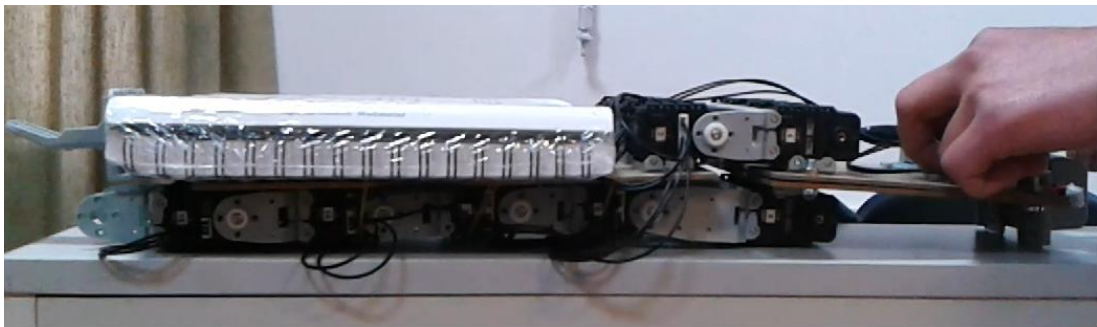


Figure 5.15: Applying 300 g load on Arm

As seen in Figure 5.16, the arm could not lift this weight by itself, and exoskeleton became a part of the action (it was activated).

In this case, the amounts of output torques of modules during weight lifting are presented in Figure 5.17. According to this graphic, while the exoskeleton was not

generating torque initially, the exoskeleton was activated when the torque of arm modules maximized so, the arm and exoskeleton lifted the weight together. At this point, the torque of arm modules decreased from 1.3 Nm to 0.55N.m, 0.62N.m, and 0.39N.m respectively and relaxed the arm, and then exoskeleton ensured lifting more weight by generating 0.7N.m and 0.67N.m torques.

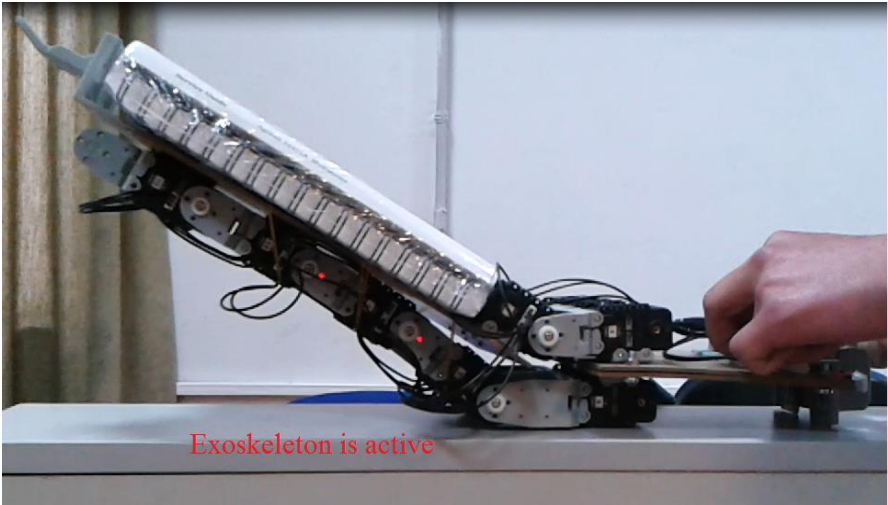


Figure 5.16: Exoskeleton is active to lift weight

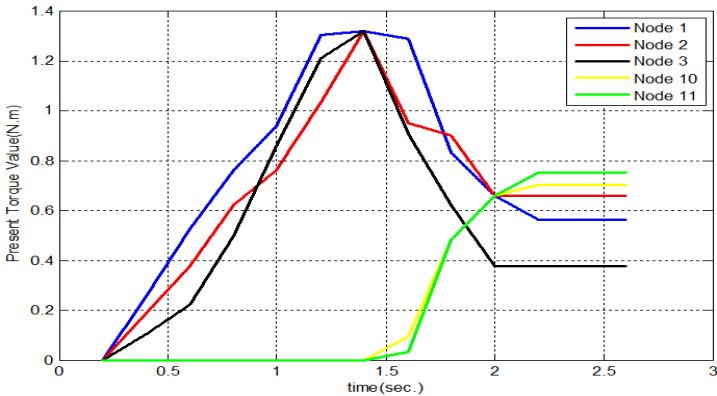


Figure 5.17: Present Torque Values on Arm and Exoskeleton Modules

Then, as seen in Figure 5.18, 2.5kg of weight is applied on arm, and it was investigated if the system can lift this weight or not.

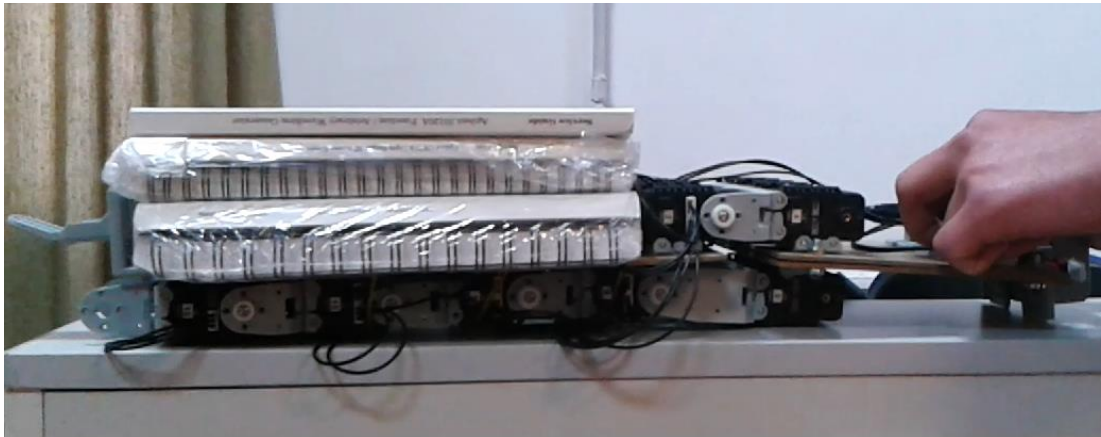


Figure 5.18: Applying 2.5kg load on Arm

The system cannot lift this weight, and the exoskeleton must perform reconfiguration in order to lift this weight.

Therefore, system has to undergo reconfiguration sequence to twist elbow part of the exoskeleton by detecting idle motors automatically. Present torque values of each exoskeleton modules are considered in order to make a decision about which node is disconnected and where it is reconnected again to lift loads and also to reach goal position. According the present torque values of each motor as shown in Figure 5.19, modules 10 and 11 reach the maximum torque capacities (1.5 N), while modules 4 and 5 produce minimum torques (0) during the experiment. So, system can chose modules 4 and 5 as idle nodes as shown in Figure 5.20. In this experiment, we disconnected to node 5 and reconnected again to between nodes 10 and 11 that have produced maximum torques.

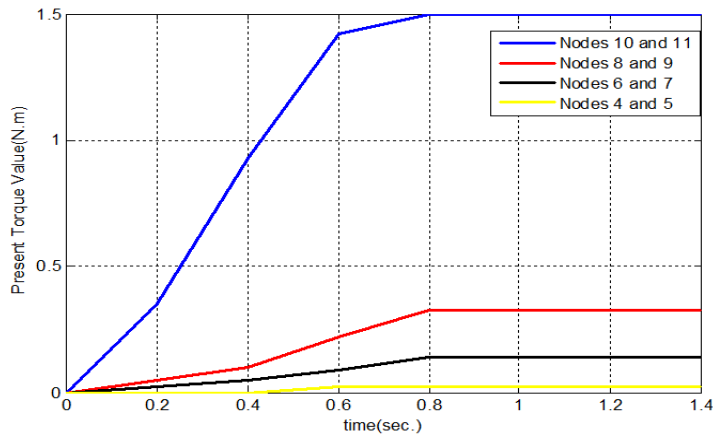


Figure 5.19: Present Torque Values on Exoskeleton Modules While Applying 2.5kg Load on Arm

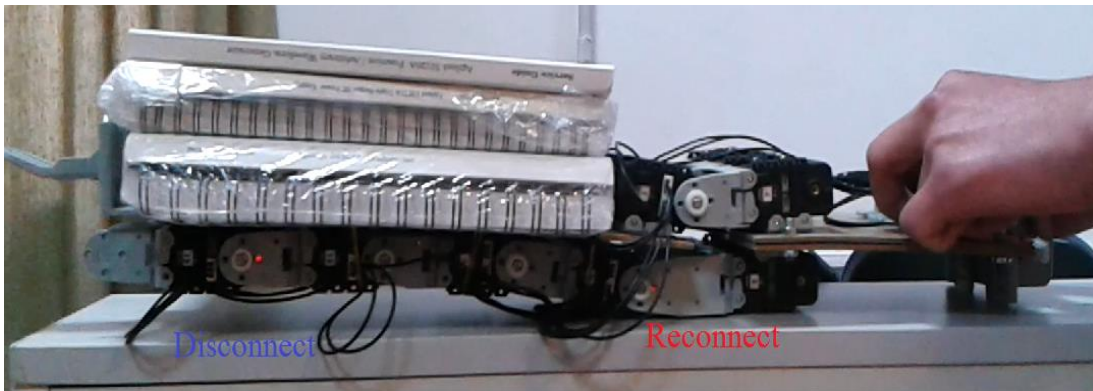


Figure 5.20: Selecting Disconnected Module for Reconfiguration

Finally, after we reconnect the module 5, we obtain the new structure as seen Figure 5.21. At new structure, modules 4, 10 and 11 are thought as exoskeleton elbow joints and these modules bend the arm together. Now, we test the new structure whether it can bend the robot arm with 3kg forces or do not.

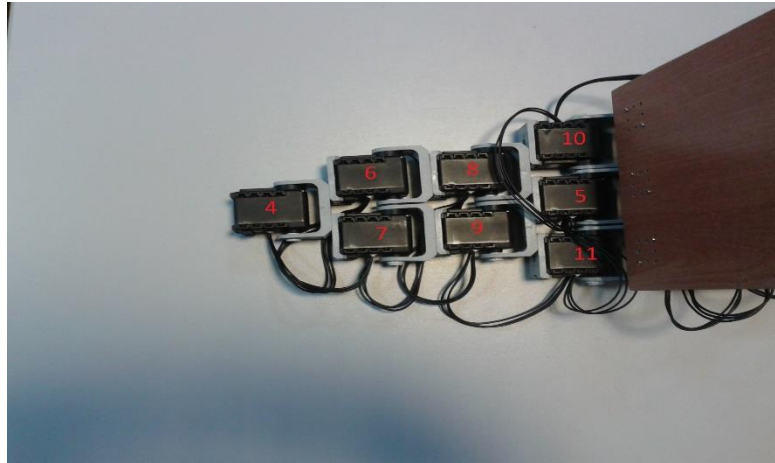


Figure 5.21: Reconfigured Exoskeleton Structure

Results obtained from Figure 5.22 shows that new structure is capable of bending the arm and modules 5, 10, and 11 produce torques which are less than the maximum torques capacities to come to target position ( $120^\circ$ ).

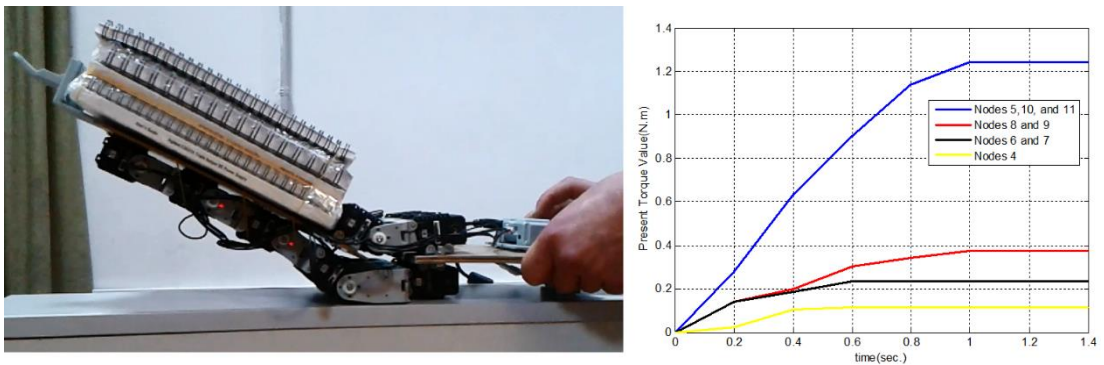


Figure 5.22: Reconfigured Exoskeleton with Present Torque Values While Lifting 2.5kg weight



## CHAPTER 6

### CONCLUSION AND FUTURE WORK

#### 6.1 Conclusions

In this thesis, we designed an adaptable modular exoskeleton undergoing a reconfiguration sequence so as to decrease an excessive load down to a range falling within the joint capabilities of the exoskeleton structure. Self-reconfiguration is based on a graph theoretic algorithm that evaluates principle eigenvector values for finding idle holons which can disconnect and the place they need to reconnect to form the new reconfiguration. Reconfigurable modular exoskeletons are found in our simulations and hardware implementations to promise being highly versatile tools that can match the body structure of a human and the changing load conditions during continuously changing activities of a human wearing the reconfigurable holonic exoskeleton. Reconfiguration is found to morph the exoskeleton meshes to the changing force needs of varying tasks.

Elapsed time between disconnecting and reconnecting for each reconfiguration sequence can be thought as reconfiguration cost. However, it is too hard to evaluate real elapsed time because, we use two computer programs separately for simulation results. Also, for hardware implementations, bioloid robots kits are not suitable like modular robots for easily disconnecting and reconnecting, so it is not possible to measure elapsed time exactly.

The exoskeleton structure created by using self-reconfigurable robots has some advantages. In such systems, the efficiency can be improved via actuators being able to produce less torque. Because, the system can find the point where the load or stress is concentrated, and they can lift the load easily by allocating the unimportant robots in the system to that location. Another advantage is that the human safety is threatened less because the actuators creating lower torques are used.

## **6.2 Further Recommendations**

In order to provide comfortable mobilization of the system mounted on the user rather than the wheelchair, exoskeleton robots' physical properties such as weight and dimensions are very important and they need to be minimized from the aspect of comfort of the disabled user. On the other hand, supporting the natural movements of any human extremity via the external mechanisms is a significantly difficult task, even though there are many exoskeleton structures available nowadays. For this reason, biomechanical assessment is crucial for the exoskeleton structures.

There is a necessity on developing the new and more effective techniques for energy resources, actuators and transmissions, because those parts are also crucial for creating an easy-to-use and portable exoskeleton robot. The safety of the human operator needs to be paid attention, because the exoskeleton robots are mounted directly on the body of user. The safety is not important by itself, because the safety of the robot in the eye of the user is more important.

Nowadays, the level of brain-machine interface technology is considerably satisfying. For this reason, while controlling the exoskeleton robot, the signals obtained from the brain can be used. So the integration between robot and the user

will be improved. It is expected in exoskeleton controlling domain to combine the signals of the brain and the muscles.

Our plan for the future is to model an arm in simulation, and to place this exoskeleton on it in the way it covers all over the arm. Then by applying the load directly to the arm, we address to determine the level of stress per link in the exoskeleton, and to control the exoskeleton according to those values. Then, model the system by removing the Ansy software, and to perform analyses on Matlab. We aim to make the node to separate and then reconnect by itself where required. So, a completely intelligent system can be provided. Designing such a system on the real system is another plan of ours. After we have full autonomous system, we can measure the reconfiguration cost exactly.



## REFERENCES

- Baca, J., Yerpes, A., Ferre, M., Escalera, J. A., Aracil, R. (2008). Modelling of Modular Robot Configurations Using Graph Theory, HAIS, Springer, pp. 649-656.
- Brown, G. W. (2011). Equiposing support apparatus. November 29 2011. US Patent 8,066,251.
- Butler, Z., Kotay, K., Rus, D., Tomita, K. (2002). Generic decentralized control for a class of self-reconfigurable robots. Proceedings 2002 IEEE International Conference on Robotics and Automation, Washington DC, pp. 809-8167
- Chen, I.-M., Burdick, J. W. (1993). Enumerating the nonisomorphic assembly configurations of modular robotic systems. Proceedings IEEE/RSJ International Conference on Intelligent Robots and Systems (IROS), Yokohama, pp. 1985–1902.
- Collins, S., Ruina, A., Tedrake, R., Wisse, M. (2005). Efficient bipedal robots based on passive-dynamic walkers. Science (New York, N.Y.), pp. 1082–1085.
- Corliss, W. R., Johnsen, E. G., (1968). Teleoperator controls an aec-nasa technology survey. Technical Report, National Aeronautics and Space Administration, Washington DC.
- Cvetkovic, D., Doob, M., Sachs, H. (1979). Spectra of Graphs, Academic Press, Inc., pp. 397-404.
- Cvetkovic, D., Rowlinson, P., Simic, S. (1997). Eigenspaces of Graphs, Cambridge University Press.

- Dollar, A. M., Herr, H. (2008). "Lower Extremity Exoskeletons and Active Orthoses: Challenges and State-of-the-Art". *IEEE Transactions on Robotics*, vol. 24, no. 1, pp. 144–158,
- Durna, M., Erkmen, A. M., Erkmen, I. (2000a). Self-localization of a holon in the reconfiguration task space of a robotic colony. *Proceedings ICRA. Millennium Conference. IEEE International Conference on Robotics and Automation*, San Francisco, CA, April, pp. 1748–1754.
- Durna, M., Erkmen, I., Erkmen, A. M. (2000b). Self-reconfiguration in task space of a holonic structure. *Proceedings. IEEE/RSJ International Conference on Intelligent Robots and Systems (IROS)*, pp. 2366–2372.
- Duysinx, P., Geradin, M. (2004). *An introduction to robotics: Mechanical Aspects*. University of Liege.
- Lenzo, B. (2013). *Design of Novel Robotic Exoskeletons with Hybrid Actuation for Human*. PhD Thesis, Scuola Superiore Sant'anna-Pisa, Innovative Technologies PhD Program.
- Frisoli, A., Bergamasco, M., Carboncini, M. C., Rossi, B. (2009). "Robotic assisted rehabilitation in Virtual Reality with the L-EXOS." *Studies in Health Technology and Informatics*, vol 145, pp. 40–54.
- Fukuda, T., Nakagawa, S., Kawauchi, Y., Buss, M. (1988). Self Organizing Robots Based on Cell Structures-CEBOT. *IEEE International Workshop on Intelligent Robots Philadelphia*, April, pp. 145–150.
- Gopura, R. (2009). *Development and Control of Upper-Limb Exoskeleton Robots*. PhD Thesis, Department of Advanced Systems Control Engineering, Graduate School of Science and Engineering, Saga University, Japan.

- He, J., Koeneman, E. J., Schultz, R. S., Herring, D. E., Wanberg, J., Huang, H. (2005). RUPERT: a Device for Robotic Upper Extremity Repetitive Therapy. IEEE Engineering in Medicine and Biology 27th Annual Conference, pp. 336–346.
- Hollerbach, J. M., Hunter, I., Ballantyne, J. (1991). "A comparative analysis of actuator technologies for robotics." *The Robotics Review* vol 2, pp. 299–342.
- Housman, S. J., Le, V., Rahman, T., Sanchez, R. J., Reinkensmeyer, D. J. (2007). Arm-Training with T-WREX After Chronic Stroke: Preliminary Results of a Randomized Controlled Trial. IEEE 10th International Conference on Rehabilitation Robotics, pp. 562–568.
- Jorgensen, M., Ostergaard, E., Lund, H. (2004). Modular ATRON: modules for a self-reconfigurable robot. IEEE/RSJ International Conference on Intelligent Robots and Systems, pp. 2068–2073.
- Khan, O. (1970). Reconfigurable Molds as Architecture Machines. Proceedings ACADIA 08, Biological Processes and Computation , pp. 286–291.
- Kazerooni, H. (2005). Exoskeletons for human power augmentation. IEEE/RSJ International Conference on Intelligent Robots and Systems, pp. 3459–3464.
- Kikuchi, T., Jin, Y., Fukushima, K., Akai, H., Furusho, J. (2008). “Hybrid-PLEMO”, rehabilitation system for upper limbs with active / passive force feedback mode. Conference Proceedings: Annual International Conference of the IEEE Engineering in Medicine and Biology Society. IEEE Engineering in Medicine and Biology Society. Conference, pp. 1973–1976.
- Kurukawa, H., Murata, S., Yoshida, E., Tomita, K., Kokaji, S. (1998). A 3-D Self-Reconfigurable Structure and Experiments. Proceedings IEEE/JRS International Conference Intelligent Robots and Systems, Victoria, BC, Canada, pp. 860-865.

- Marcheschi, S., Salsedo, F., Fontana, M., Bergamasco, M. (2011). Body Extender: Whole body exoskeleton for human power augmentation. IEEE International Conference on Robotics and Automation, pp. 611–616.
- Mark, Yim, Paul, W., Park, M., SASTRA, J. (2009). Modular Self-Reconfigurable Robots, Encyclopedia of Complexity and Systems Science, Springer, pp. 19–33.
- Mehrabi, M.G., Ulsoy, A.G. & Koren, Y. (2000). "Reconfigurable manufacturing systems: key to future manufacturing." Journal of Intelligent Manufacturing, vol.11, pp.403–419.
- Murata, S. (1994). Self-Assembling Machine. Proceedings IEEE International Conference Robotics and Automation, San Diego, pp.441-448.
- Ragonesi, D., Agrawal, S., Sample, W., Rahman, T., Wrex, A. M. (2011). Series Elastic Actuator Control of a Powered Exoskeleton. Proceedings 33<sup>rd</sup> Annual International Conference of the IEEE, EMBS, Boston, pp. 3515–3518.
- Rus, D., Vona, M. (2000). A physical implementation of the self-reconfiguring crystalline robot. Proceedings 2000 ICRA. Millennium Conference. IEEE International Conference on Robotics and Automation. Symposia (ICRA), San Francisco, April, pp. 1726–1733.
- Sanchez, R. J., Liu, J., Rao, S., Shah, P., Smith, R., Rahman, T., Reinkensmeyer, D. J. (2006). "Automating arm movement training following severe stroke: functional exercises with quantitative feedback in a gravity-reduced environment." IEEE Transactions on Neural Systems and Rehabilitation Engineering: A Publication of the IEEE Engineering in Medicine and Biology Society, vol. 14, no. 3, pp. 378–389.
- Sankai, Y. (2011). Hal: Hybrid assistive limb based on cybernics. Robotics Research, Springer, pp. 25–34.

- Strausser, K. A., Kazerooni, H. (2011). The development and testing of a human machine interface for a mobile medical exoskeleton. *IEEE/RSJ International Conference on Intelligent Robots and Systems*, pp. 4911–4916.
- Veneman, J. F., Kruidhof, R., Hekman, E., Ekkelenkamp, R., Van Asseldonk, E. H., van der Kooij, H. (2007). "Design and evaluation of the LOPES exoskeleton robot for interactive gait rehabilitation." *IEEE Transactions on Neural Systems and Rehabilitation Engineering*, vol. 15, no. 3, pp. 379–386.
- Wang, R. J., Huang, H. P., Lee, P. T., Liao, H. F. (2012). " Avertically intersected dual-axis modularized reconfigurable actuator: design and application for a six-axis humanoid robot arm." *Journal of the Chinese Institute Of Engineers*, vol. 36, no. 4, pp. 530-541
- Wang, S., van Dijk, W., van der Kooij, H. (2011). Spring uses in exoskeleton actuation design. *Proceedings in Rehabilitation Robotics (ICORR), IEEE International Confererance*, pp. 1-6.
- Yim, M., Duff, D. G., Roufas, K. D. (2000). PolyBot: a modular reconfigurable robot. *Proceedings 2000 ICRA. Millennium Conference. IEEE International Conference on Robotics and Automation. Symposia, San Francisco, April*, pp. 514–520.
- Zoss, A., Kazerooni, H., Chu, A. (2006). "Biomechanical design of the Berkeley lower extremity exoskeleton (BLEEX)." *IEEE/ASME Transactions on Mechatronics*, vol. 11, no. 2, pp. 128–138.